Isotopic evidence for complex biogeochemical cycling of Cd in the eastern tropical South Pacific

Ruifang C. Xie
GEOMAR Helmholtz Center for Ocean Research Kiel, Wischhofstrasse 1-3, D-24148 Kiel, Germany
rxie@geomar.de

Mark Rehkämper
Department of Earth Science and Engineering, Imperial College London, London SW7 2AZ, UK
markrehk@imperial.ac.uk

Patricia Grasse
GEOMAR Helmholtz Center for Ocean Research Kiel, Wischhofstrasse 1-3, D-24148 Kiel, Germany
pgrasse@geomar.de

Tina van de Flierdt
Department of Earth Science and Engineering, Imperial College London, London SW7 2AZ, UK
tina.vandeflierdt@imperial.ac.uk

Martin Frank
GEOMAR Helmholtz Center for Ocean Research Kiel, Wischhofstrasse 1-3, D-24148 Kiel, Germany
mfrank@geomar.de

Zichen Xue
Department of Earth Science and Engineering, Imperial College London, London SW7 2AZ, UK
zichenxue@gmail.com

Keywords: dissolved Cd stable isotopes, eastern tropical South Pacific, oxygen minimum zone, steady state fractionation model, Cd depletion

Abstract

Over the past decades, observations have confirmed decreasing oxygen levels and shoaling of oxygen minimum zones (OMZs) in the tropical oceans. Such changes impact the biogeochemical cycling of micronutrients such as Cd, but the potential consequences are only poorly constrained. Here, we present seawater Cd concentrations and isotope compositions for 12 depth profiles at coastal, nearshore and offshore stations from 4ºS to 14ºS in the eastern tropical South Pacific, where one of the world's strongest OMZs prevails.

The depth profiles of Cd isotopes display high $\delta^{114/110}$Cd at the surface and decreasing $\delta^{114/110}$Cd with increasing water depth, consistent with preferential utilization of lighter Cd isotopes during biological uptake in the euphotic zone and subsequent remineralization of the sinking biomass. In the surface and subsurface ocean, seawater displays similar $\delta^{114/110}$Cd signatures of 0.47 ±0.23‰ to 0.82±0.05‰ across the entire eastern tropical South Pacific despite highly variable Cd concentrations between 0.01 and 0.84 nmol/kg. This observation, best explained by an open system steady-state fractionation model, contrasts with previous studies of the South Atlantic and South Pacific Oceans, where only Cd-deficient waters have a relatively constant Cd isotope signature. For the subsurface to about 500 m depth, the variability of seawater Cd isotope compositions can be modeled by mixing of remineralized Cd with subsurface water from the base of the mixed layer. In the intermediate and deep eastern tropical South Pacific (> 500 m), seawater [Cd] and $\delta^{114/110}$Cd appear to follow the distribution and mixing of major water masses. We identified modified AAIW of the ETSP to be more enriched in [Cd] than AAIW from the source region, whilst both water masses have similar $\delta^{114/110}$Cd. A mass balance estimate thus constrains a $\delta^{114/110}$Cd of between 0.38‰ and 0.56‰ for the accumulated remineralized Cd in the ETSP.

Nearly all samples show a tight coupling of Cd and PO_4 concentrations, whereby surface and deeper waters define two distinct linear trends. However, seawater at a coastal station located within a pronounced plume of H_2S, is depleted in [Cd] and features significantly higher $\delta^{114/110}$Cd.

61 This signature is attributed to the formation of authigenic CdS with preferential incorporation of
62 lighter Cd isotopes. The process follows a Rayleigh fractionation model with a fractionation factor
63 of $\alpha^{114/110}Cd_{seawater\text{-}CdS} = 1.00029$. Further deviations from the deep Cd-PO_4 trend were observed
64 for samples with $O_2 < 10$ μmol/kg and are best explained by in situ CdS precipitation within the
65 decaying organic matter even though dissolved H_2S was not detectable in ambient seawater.
66

Highlights

- Constant surface $\delta^{114/110}Cd$ is best described by a steady-state model
- Large Cd isotope fractionation due to CdS precipitation in the euxinic Peruvian OMZ
- OMZ Cd-PO_4 decoupling attributed to remineralization-induced CdS formation
- Relative to Southern Ocean AAIW, modified AAIW in the ETSP has twice as much Cd but similar $\delta^{114/110}Cd$
- Water mass control on intermediate and deep water $\delta^{114/110}Cd$ distribution in the ETSP

1. Introduction

The oceanic cycling of dissolved Cd is enigmatic. Whilst low levels of dissolved Cd in the surface ocean generally do not appear to limit marine phytoplankton growth, seawater Cd concentrations show a nutrient-like distribution, which resembles that of the macronutrient phosphate (e.g., Boyle et al., 1976). Although the mechanisms of Cd removal from surface waters are debated (Horner et al., 2013a, 2013b; Morel 2013), the biological function of Cd in the marine environment is clear in some cases. In particular, Cd was shown to promote phytoplankton growth by substituting Zn in Zn-specific carbonic anhydrase under Zn-limiting conditions (e.g., Price and Morel, 1990). The discovery of a Cd-specific carbonic anhydrase in *T. weissflogii* further supports a metabolic role of Cd in some species (Lane and Morel, 2000).

The biological function of Cd is further supported by recent studies on marine Cd isotopes (e.g., Abouchami et al., 2011; Lacan et al., 2006; Ripperger et al., 2007). In the surface ocean, seawater generally has more positive $\delta^{114/110}$Cd values that decrease with depth (Abouchami et al., 2011; Abouchami et al., 2014; Ripperger et al., 2007). This is in line with culturing experiments that revealed preferential assimilation of light Cd isotopes during biological uptake (John and Conway, 2014; Lacan et al., 2006), although the seawater (SW)-biomass isotope fractionation factors α observed in these experiments for ^{114}Cd/^{110}Cd were much higher, at $\alpha^{114/110}Cd_{SW\text{-}biomass}$ = 1.0008 to 1.0014, than those observed in the global ocean ($\alpha^{114/110}Cd_{SW\text{-}biomass}$ = 1.0002 to 1.0004; e.g. Abouchami et al., 2014; Xue et al. 2013). This difference in isotope fractionation has been ascribed to differences in the phytoplankton uptake pathways at low *vs.* high Cd concentrations (Conway and John, 2015a).

The mechanisms governing Cd isotope fractionation during biological uptake in the surface ocean seem to vary spatially and temporally. In the Southern Ocean and part of the North Pacific, the evolution of seawater $\delta^{114/110}$Cd in the upper water column appears to closely follow a Rayleigh fractionation model (Abouchami et al., 2011; 2014; Janssen et al., 2017; Xue et al., 2013; Yang et al., 2018), whereby Cd is continuously removed from the system. Conversely, Xie et al.

(2017) suggested that global Cd-deficient seawater, regardless of location, has a relatively uniform $\delta^{114/110}$Cd of +0.4‰ to +1.0‰ that can be explained by a steady state model, in which the export of Cd out of the surface ocean is balanced by the input via upwelled Cd-rich seawater. This inference was recently corroborated by a Cd isotope study along the meridional GEOTRACES GP19 section in the South Pacific (Sieber et al., 2019). Alternatively, Xie et al. (2017) proposed that, if Rayleigh fractionation indeed governs Cd isotope fractionation in Cd-deficient surface waters, the low and homogeneous $\delta^{114/110}$Cd values may reflect that >85% of the dissolved Cd budget is buffered by ligand complexation. Recent studies also showed that physical processes such as water mass advection or the temporal presence of eddies may determine if Cd uptake follows Rayleigh or steady state fractionation trends (Janssen et al., 2017; Yang et al., 2018). Furthermore, a supply-limited model was proposed to explain the relatively small Cd isotope fractionations observed for Cd-depleted surface waters off the east coast of New Zealand (Gault-Ringold et al., 2012).

The processes that control the distribution of Cd isotopes in deep waters are more straightforward. Deep Pacific and Southern Oceans waters are characterized by a relatively constant $\delta^{114/110}$Cd ≈ +0.26‰ (Abouchami et al., 2014; Janssen et al., 2017; John et al., 2018; Sieber et al., 2019; Xue et al., 2013; Yang et al., 2018), while the deep Atlantic Ocean features a north-south contrast between more fractionated North Atlantic Deep Water (NADW, $\delta^{114/110}$Cd ≈ +0.42‰) and less fractionated Antarctic Bottom Water (AABW, $\delta^{114/110}$Cd ≈ +0.24‰) (Xie et al., 2017). This quasi-conservative behavior of Cd isotopes allows the use of $\delta^{114/110}$Cd as a reliable water mass tracer in the intermediate and deep Atlantic, at least in the modern ocean (Abouchami et al., 2014; Sieber et al., 2019; Xie et al., 2017; Xie et al., 2019).

In contrast, the distribution of Cd and Cd isotopes in oxygen-deficient waters does not appear to follow a pattern defined by biological utilization or water mass mixing. Cadmium depletion relative to PO_4 in these waters was reported for the upper part of oxygen minimum zones (OMZs) in the northeast subarctic Pacific (Janssen et al., 2014) and the eastern subtropical Atlantic (Conway and John, 2015a; Janssen et al., 2014; Waeles et al., 2013, 2016). This depleted Cd

127 signal was attributed to authigenic CdS precipitation within microenvironments of decaying
128 organic matter, which host a sulfate reducing core that provides free H_2S to bind Cd (Bianchi et
129 al., 2018). This process appears to preferentially incorporate lighter Cd isotopes into the solid
130 phase, as shown by analyses of sulfidic minerals (Schmitt et al., 2009), ab initio calculations
131 (Yang et al., 2016), and precipitation experiments (Guinoiseau et al., 2018). Indeed, particulates
132 from such low-oxygen waters are characterized by relatively low $\delta^{114/110}Cd \approx 0‰$ (Janssen et al.,
133 2014). However, Cd depletions do not appear to be a ubiquitous feature for all low-oxygen marine
134 environment (John et al., 2018; Yang et al., 2018).
135 The eastern tropical South Pacific (ETSP) hosts one of the world's largest OMZ, but data
136 on dissolved Cd isotopes are scarce. A recent study on samples from the GEOTRACES GP16
137 section reported slight Cd depletions relative to PO_4 at nearshore and offshore stations off Peru,
138 which might be related to changes in ecological communities (John et al., 2018). As such, it
139 remains unclear whether low oxygen waters of the ETSP OMZ act as a sink for light Cd isotopes
140 within the water column, which is not only important for an improved understanding of
141 micronutrient cycling in the present day ocean but will also allow more reliable reconstructions of
142 oxygen depleted marine paleoenvironments. This study systematically investigates the
143 biogeochemical cycling of Cd and its isotopes within the ETSP, with particular focus on the Cd
144 isotope fractionation in an oxygen depleted water column, the Cd-PO_4 correlation within anoxic
145 and sometimes sulfidic subsurface waters, and the importance of water mass mixing for the
146 distribution of Cd isotopes.
147
148 **2. Sampling and analytical methods**
149 *2.1 Sampling*
150 Seawater was sampled during two back-to-back cruises on board of the German research
151 vessel Meteor from Guayaquil (Ecuador) to Callao (Peru) in January 2009 (M77/3) and from
152 Callao to Colon (Panama) in February 2009 (M77/4) (Fig. 1a). In total, 82 samples were collected

153 from 12 depth profiles covering the full range of low oxygen waters between 4°S and 14°S along
154 two semi-meridional transects at 86°W and 82°W, and along a coastal transect; these encompass
155 three coastal, four nearshore and five offshore stations (Fig. 1).

156 All samples were collected using ultraclean GO-FLO bottles mounted on a plastic coated
157 rosette system and deployed with a Kevlar cable. Upon return of the rosette system, samples were
158 immediately filtered through 0.45 μm Millipore cellulose acetate filters into acid-cleaned
159 polyethylene canister/bottles and acidified to pH ~2 using distilled 12 M HCl inside a Class-5
160 clean room container. All sample bottles were double-bagged and shipped to the home laboratory.
161

162 *2.2 Analytical Methods*

163 The methods for the acquisition of oxygen and phosphate concentrations are described
164 elsewhere (Grasse et al., 2016). Salinity and potential temperature were retrieved from the CTD
165 sensors. The separation and isotopic analysis of Cd were carried out at the Imperial College
166 MAGIC Laboratories following Ripperger and Rehkämper (2007) and Xue et al. (2012), and only
167 a brief summary of methods is provided here. For samples with [Cd] ≥ 0.1 nmol/kg, 0.3 to 3 L of
168 seawater containing ~30 ng of Cd were weighed and spiked with a ^{111}Cd-^{113}Cd tracer to a ratio of
169 spike to natural Cd of ~1. Cadmium was then extracted from the seawater using a three-stage
170 column chemistry procedure (Xue et al., 2012). For seawater samples with [Cd] < 0.1 nmol/kg,
171 sample volumes of 3 to 20 L were weighed and spiked. Cadmium from these samples was first
172 extracted by co-precipitation with $Al(OH)_3$, followed by purification using the standard column
173 chemistry procedure (Xue et al., 2012).

174 The Cd isotope compositions were measured on a Nu Plasma HR multiple collector
175 inductively coupled plasma mass spectrometer (MC-ICP-MS), following established methods
176 (Ripperger and Rehkämper, 2007; Xue et al., 2012). The stable Cd isotope compositions of the
177 samples are expressed as $\delta^{114/110}$Cd values relative to the NIST SRM 3108 isotope standard (std)
178 (Abouchami et al., 2013):

$$\delta^{114/110}\text{Cd}\ (‰) = \left(\frac{(^{114}Cd/^{110}Cd)_{sample}}{(^{114}Cd/^{110}Cd)_{std}} - 1\right) \times 1000$$

The secondary Cd isotope standards BAM-I012 Cd, JMC Cd Münster, and Alfa Cd Zurich were routinely analyzed alongside with the seawater samples (Xue et al., 2012) and yielded results identical, within error, to the reference values (Abouchami et al., 2013). The total procedural Cd blank was ~20 pg per sample, which corresponds to a maximum contribution of ~0.05% to the total Cd present in the sample aliquots. The blank was subtracted from the measured sample [Cd] data but no corrections were applied to $\delta^{114/110}$Cd results, as the isotope composition of the blank was not well defined.

3. Results

3.1 Hydrographic Setting off Peru

Surface waters (upper 10 m) in the study area show a wide range of temperatures (15°C to 27°C) and salinities (34.4 to 35.6; Figs. 1b, 2). Accordingly, surface waters at offshore stations can be divided into Equatorial Surface Water (ESW: T<25°C, Sal. >34) influencing Sts. 109 and 134, and Subtropical Surface Water (STSW: Sal. >35), present at Sts. 86, 93 and 97 (Sal. > 35; Fiedler and Talley, 2006; Fig. 2). The STSW, originating from the eastern flank of the subtropical gyre, is a highly oxygenated water mass found both in the mixed layer and upper thermocline off Peru (Silva et al., 2009). Nearshore and coastal stations (Sts. 11, 19, 78, 117, 120, 122, and 124) are strongly influenced by upwelling of cold and nutrient-rich subsurface waters, the so-called Equatorial Subsurface Water (ESSW: T =12.5°C; Sal. = 34.9; σ_θ =26 kg/m^3; Silva et al., 2009; Fig. 2). The ESSW is carried southward within the Peru Chile Undercurrent (PCUC; Fig. 1b), which is partly fed by the Equatorial Undercurrent (EUC) and the Southern Subsurface Countercurrent (SSCC; e.g., Fiedler and Talley, 2006). In its southward flow path, the PCUC alters its biochemical properties due to enhanced remineralization within the OMZ and processes at the seawater-sediment boundary (e.g., Bruland et al., 2005). In the same density range as the ESSW but at a distance from the continental slope, the Shallow Salinity Minimum Water

205 (SSMW), characterized by a distinct salinity minimum at σ_θ = 26 kg/m^3 (Karstensen, 2004),
206 influences the southernmost offshore stations (Sts. 86, 93 and 97).

207 Intermediate water masses (500 m to 1200 m) in the study area mainly consist of
208 Equatorial Pacific Intermediate Water (EqPIW), whereas stations in the south (Sts. 78, 86, and 93)
209 show admixture of Antarctic Intermediate Water (AAIW) characterized by lower salinities (34.3 to
210 34.5). Below AAIW, Pacific Deep Water (PDW) has a broad silicate maximum (up to 160
211 µmol/kg, σ_θ > 27.5 kg/m^3) centered at depths between 1200 and 3000 m. The PDW arrives in this
212 region following an intricate path through the North Pacific and is thought to be the return flow of
213 modified bottom waters originating from the South Pacific in the Antarctic Circumpolar Current
214 (ACC) (Llanillo et al., 2013; Reid, 1973; Tsuchiya and Talley, 1998). The densest water mass of
215 the study area derives from the Southern Ocean and is a mixture of Lower Circumpolar Deep
216 Water (LCDW) and the underlying Antarctic Bottom water (AABW; Kawabe and Fujio, 2010),
217 whereby the latter is characterized by a salinity maximum and a silicate minimum. According to
218 the salinity data, only St. 93 shows week admixture of LCDW at depth.
219
220 ***3.2 Depth profiles of Cd and $\varepsilon^{114/110}$Cd along with oxygen and PO_4***
221 The vertical profiles of [Cd] and $\delta^{114/110}$Cd (Table 1) are presented along with oxygen and
222 PO_4 concentrations in Figs. 3 and S1 (see supplementary material). The ETSP is characterized by a
223 pronounced OMZ with oxygen concentrations in the core of the OMZ generally below 10
224 µmol/kg. The extent of the OMZ varies between stations. At coastal stations (Sts. 122 and 19), the
225 water column is anoxic below 20 m depth. The largest extent of the OMZ, between approximately
226 50 m and 400 m in depth, occurs at nearshore stations (Sts. 117, 124, 11, and 78), whereas at
227 offshore stations (Sts. 109, 134, 97, 93, and 86) the OMZ ranges from about 150 m to 400 m depth
228 (Fig. 3). In the following, waters with O_2 < 10 µmol/kg are defined as oxygen minimum waters,
229 and the sharp decline in [O_2] above the OMZ as the upper oxycline.

Cadmium concentrations in surface waters within the Peruvian OMZ are more depleted at the offshore stations ([Cd] = 0.01 – 0.04 nmol/kg) and increase towards the coast where [Cd] reaches values up to 0.63 nmol/kg. Conversely, surface waters at all stations have relatively constant $\delta^{114/110}$Cd of 0.47‰ to 0.82‰, which are within, or almost within, error of each other. No discernable trend in surface water $\delta^{114/110}$Cd is observed between the offshore, nearshore, and coastal stations.

At offshore (Sts. 109, 134, 97, 93, and 86) and nearshore (Sts. 117, 124, 11, and 78) stations (Fig. 3), the vertical variations of [Cd] closely match those of [PO_4] (no PO_4 data are available for Sts. 78 and 86). Below the surface, both Cd and PO_4 concentrations increase rapidly within the upper oxycline where O_2 drops below 50 μmol/kg (4ºS and 6ºS) or below detection limit (12ºS and 14ºS) (Fig. 3). Just below the upper oxycline, the increase in [Cd] is interrupted by a pause at the northern stations at 4ºS and 6ºS, or a shift of up to 0.1 nmol/kg toward lower [Cd] at the southern stations at 12ºS and 14ºS. These slight decreases in [Cd] are accompanied by more slowly increasing [PO_4]. A more gradual increase in [Cd] and [PO_4] is observed within the OMZ, followed by only a slight increase below the OMZ. Maxima of [Cd] and [PO_4] are seen at these stations between depths of 500 and 1500 m (Fig. S1).

At nearshore locations, a sharp decrease in $\delta^{114/110}$Cd from the surface to ~200 m is observed at most stations, which matches the rapid increase in [Cd] and the decrease in O_2 (Figs. 3 and S1). Below ~200 m, $\delta^{114/110}$Cd slowly decrease to values typical for deep Southern and Pacific Ocean waters. At the offshore stations, the sharp subsurface decrease in $\delta^{114/110}$Cd is not evident except at St. 109 at 4ºS. Instead, these stations display a gradual decrease in $\delta^{114/110}$Cd with depth.

At coastal stations (Fig. 3), where the upper oxycline only occupies a very shallow depth of 20-40 m, vertical trends of [Cd] and $\delta^{114/110}$Cd at 4ºS and 6ºS are similar to those at the offshore and nearshore stations, with perhaps a smaller vertical [Cd] gradient due to intense upwelling. At St. 19 at 12ºS, however, [Cd] decreases drastically with depth, whilst $\delta^{114/110}$Cd increases from

0.65‰ at the surface to 1.3‰ at 60 m. The latter depth corresponds to the center of a large H_2S plume (30 – 100 m water depth) at the time of sampling (Schunck et al., 2013).

Although the sampling program did not include a direct crossover station with the GEOTRACES program, our new Cd and $\delta^{114/110}$Cd data for Sts. 11 and 97 at 12ºS show excellent agreement with results obtained for samples from the nearby Sts. 4, 5 and St. 7, respectively, of the GEOTRACES P16 transect (Fig. S2; see supplementary material) (John et al., 2018). Minor differences of up to 60 pmol/kg (240 pmol/kg at the surface) in [Cd] and up to 0.25‰ in $\delta^{114/110}$Cd are evident between the datasets but these likely reflect inter-annual variability, particularly at the surface.

4. Discussion

Biological control on the vertical distribution of Cd and Cd isotopes in the Peruvian upwelling region is evident in the [Cd] and $\delta^{114/110}$Cd profiles (Figs. 3 and S1). Low [Cd] coupled with high $\delta^{114/110}$Cd values in the surface waters suggests preferential uptake of light Cd isotopes during phytoplankton growth, while higher [Cd] and lower $\delta^{114/110}$Cd in deeper waters result from remineralization of sinking biomass. These systematics are comparable to those seen in the western (e.g. Abe, 2002; Boyle et al., 1976; Sieber et al., 2019; Yang et al., 2018) and eastern Pacific (e.g. Bruland et al., 1978; Conway and John, 2015b; Janssen et al., 2017; John et al., 2018). However, the shapes of the [Cd] and $\delta^{114/110}$Cd profiles of this study are clearly affected by the vertical distribution of oxygen, whereby the most rapid increases in [Cd], and thus rapid decreases in $\delta^{114/110}$Cd, are restricted to the upper oxycline. The maximum concentrations of Cd and PO_4 observed at mid-depth in our study and others most likely reflect maximum remineralization of organic matter in the epipelagic (0 - 200 m) and mesopelagic (200 - 1000 m) regions (Henson et al., 2012).

Aside from that, however, the vertical profiles of [Cd] and $\delta^{114/110}$Cd in this region show distinct features that cannot be reconciled with a simple one-dimensional biological uptake-

281 remineralization model. In the following, we explore processes that may be responsible for the
282 near-constant $\delta^{114/110}$Cd values of surface and subsurface waters, the small but significant [Cd]
283 decrease in the OMZ compared to non OMZ profiles, and the water mass control on Cd isotopes in
284 the Peruvian upwelling region.
285
286 **4.1 Biological control on upper-ocean Cd isotope systematics**
287 **4.1.1 Steady-state Cd isotope fractionation in surface waters**
288 A striking feature of the present dataset is that as surface water [Cd] decreases from coastal
289 to offshore stations, seawater Cd isotope compositions remain relatively constant, ranging between
290 $\delta^{114/110}$Cd = 0.47±0.23‰ and 0.82±0.05‰ (2SE; Fig. 3, Table 1). In particular, $\delta^{114/110}$Cd values in
291 the top 100 m, as well as the top 200 m for the offshore stations from 6º to 14 ºS, are identical
292 within error. This suggests that biological uptake of Cd does not generate large isotope
293 fractionation in this region, regardless whether the waters have high or low Cd contents. This
294 stands in contrast to previous studies of the North Atlantic and North Pacific, where highly
295 fractionated $\delta^{114/110}$Cd values were reported (Conway and John, 2015a; Ripperger et al., 2007).
296 Furthermore, the relatively constant surface $\delta^{114/110}$Cd values are at odds with dissolved Si isotope
297 distributions ($\delta^{30}Si(OH)_4$) for largely the same samples from the same cruises in the Peruvian
298 OMZ. The latter samples display large Si isotope differences as surface water [Si] decreases from
299 coastal to offshore stations, due to intense biological uptake by diatoms, and advection and mixing
300 of different water masses with distinct $\delta^{30}Si(OH)_4$ signatures (Grasse et al., 2013). The different
301 behavior of surface water $\delta^{114/110}$Cd and $\delta^{30}Si(OH)_4$ likely reflects different processes that control
302 Cd and Si isotope fractionation during biological assimilation. While the distribution of
303 $\delta^{30}Si(OH)_4$ in the Peruvian OMZ tends to closely follow a closed-system Rayleigh fractionation
304 model (Grasse et al., 2016), and although seawater Cd isotope data from the Southern Ocean
305 (Abouchami et al., 2011; Abouchami et al., 2014; Xue et al., 2013) and part of the North Pacific
306 (Janssen et al., 2017; Ripperger et al., 2007; Yang et al., 2018) are also best explained by Rayleigh

fractionation, such a model appears to be less suitable for the biogeochemical cycling of Cd in the Peruvian OMZ.

Water mass mixing at the surface may adequately explain the large west-east [Cd] gradient seen in the Peruvian OMZ (Fig. 2). At the coastal and nearshore stations, upwelled waters are primarily sourced from the PCUC, which prevails at depths of 50 – 100 m at ~ 5ºS but deepens to ~ 150 – 200 m at 10°S (Huyer et al., 1987; Penven et al., 2005). The upwelled nutrient-rich waters are subsequently transported westward to the offshore stations. Along their westward flow, Cd is continuously removed from the surface water during biological uptake. Surface water masses originating from the equatorial and central Pacific may, furthermore, have different preformed [Cd]. However, it remains elusive why different surface water masses have essentially the same $\delta^{114/110}$Cd. Note that these systematics differ from those observed along the Zero Meridian in the Southern Ocean (Abouchami et al., 2011; Xue et al., 2013) where surface biological drawdown in [Cd] is accompanied by increasing $\delta^{114/110}$Cd.

Possible explanations for the relatively constant surface $\delta^{114/110}$Cd signature include supply-limited diffusion of Cd through cells, which results in no apparent Cd isotope fractionation (Gault-Ringold et al. 2012), and Cd-ligand complexation, which buffers surface water $\delta^{114/110}$Cd to low values (Xie et al., 2017). Yet, these hypotheses are based on Cd isotope data from Cd-depleted waters and cannot explain why some Cd-replete surface waters of the Peruvian OMZ have $\delta^{114/110}$Cd similar to the global Cd isotope dataset at low [Cd] levels, as seen in supplementary Fig. S3.

The relatively constant Cd isotope signature for surface and subsurface waters (top 100 - 200 m), characterized by high O_2 and low potential densities, can be explained by an open system steady-state fractionation model (Fig. 4). This is in line with previous studies of the South Pacific (Gault-Ringold et al., 2012; Sieber et al., 2019), the North Pacific (Janssen et al., 2017) and the South Atlantic (Xie et al., 2017). Addition of the new Cd isotope data from the Peruvian upwelling zone to the global compilation (Fig. S3), suggests that a homogeneous surface water signature of

$\delta^{114/110}$Cd ≈ 0.4‰ to 1.0‰ is likely a common feature of the global oceans and that global Cd isotope systematics are possibly governed by steady state fractionation. A few deviations from the steady-state model at very low [Cd] in Fig. S3 might reflect real oceanic features. But these highly fractionated values were also only measured using MC-ICP-MS and are not from TIMS analyses, and thus may reflect potential artifacts of the MC-ICP-MS technique (Janssen et al., 2017; Xie et al., 2017).

The calculation of surface water Cd isotope compositions as a function of [Cd] for the steady-state model requires an initial estimate for [Cd] and $\delta^{114/110}$Cd of the source waters that are upwelled to the surface layer (Ripperger et al., 2007; Xie et al., 2017). Here, we choose two distinct starting compositions, based on the average values observed for northern nearshore stations at 4º and 6°S for water depths between 40 and 150 m (with [Cd] = 0.63 nmol/kg, $\delta^{114/110}$Cd = 0.54‰) and for depths between 150 and 200 m depth ([Cd] = 0.71 nmol/kg, $\delta^{114/110}$Cd = 0.57‰) at southern stations at 12º and 14°S (Fig. 4a). This practice assumes that changes in source water Cd isotope compositions and seawater-biomass fractionation factors (of $\alpha^{114/110}Cd_{SW\text{-}biomass}$ = 1.0001 to 1.0004) best explain the evolution of [Cd] and $\delta^{114/110}$Cd in surface and subsurface waters (Xue et al., 2013; Xie et al., 2017). Although this one-dimensional model ignores lateral advection and atmospheric inputs, and is hence an oversimplification, it provides a simple mechanism, which is able to account for the Cd isotope fractionation that accompanies biological uptake in many parts of the surface oceans.

4.1.2 Remineralization-mediated intermediate water Cd isotope fractionation

The vertical increase in [Cd] with increasing depth is tightly coupled to elevated [PO_4] (Fig. 3), and is thus likely a result of in situ remineralization. Indeed, the concomitant variations of Cd and $\delta^{114/110}$Cd highlight the importance of remineralization for the distribution of Cd and Cd isotopes in intermediate waters. As such, the evolution of subsurface and intermediate water $\delta^{114/110}$Cd values with increasing [Cd] at depth can be modeled by adding remineralized Cd to

359 subsurface waters, to produce binary mixing curves between these two endmembers (Fig. 4b; see
360 supplementary material). The calculated mixing lines for mixing between remineralized and
361 preformed seawater Cd (Fig. 4b) cover a large range of [Cd] and $\delta^{114/110}$Cd values and although the
362 model oversimplifies the biogeochemical processes of the Peruvian upwelling region, it can
363 account for the observed intermediate water [Cd] and Cd isotope distribution. Future studies that
364 include coupled analyses of seawater and particulate samples are desirable in this context to
365 improve understanding of Cd isotope fractionation during remineralization.
366
367 **4.2 The origin(s) of Cd-PO_4 decoupling in the OMZ**
368 A cross plot of Cd versus PO_4 concentrations (Fig. 5) highlights that processes other than
369 utilization and remineralization also play an important role in the biogeochemical cycling of Cd
370 within the Peruvian OMZ. Specifically, seawater samples from this study exhibit two distinct
371 linear trends between Cd and PO_4 – one trend for surface waters with PO_4 < 1.5 μmol/kg that is
372 defined by [Cd] = (0.18 ± 0.02)[PO_4] – (0.06 ± 0.02) (r^2 = 0.87), and a second one for subsurface,
373 intermediate and deep waters with PO_4 > 1.5 μmol/kg defined by [Cd] = (0.32 ± 0.02)[PO_4] –
374 (0.01 ± 0.05) (r^2 = 0.89). The slopes of these trends agree well with slopes (~0.27 nmol/μmol to
375 0.36 nmol/μmol) reported previously for Pacific seawater (Cullen, 2006; de Baar et al., 1994; and
376 references therein). The subsurface to deep water Cd-PO_4 relationship of this study appears to
377 show a slight offset towards higher [PO_4] from the trend of the GEOTRACES P16 transect (John
378 et al., 2018); however, the slopes defined by the two datasets are identical within error.
379 Importantly, there are clear deviations from the linear subsurface to deep water Cd-PO_4
380 correlation of this study. Specifically, these are (1) Cd enrichment relative to PO_4 at St. 122; (2)
381 minor depletion of Cd relative to PO_4 for OMZ samples with O_2 < 10 μmol/kg; and (3) a strong
382 depletion of Cd relative to PO_4 at St. 19.
383 The Cd enrichment in bottom water samples of St. 122 most likely reflects oxidation and
384 release of sedimentary Cd. The organic-rich anoxic sediments underlying upwelling areas at

continental margins, such as the Peruvian margin, are important sinks for redox-sensitive elements (e.g., Fe) and sulfide forming trace metals such as Cd. But more importantly, the preservation of organically-bound Cd is greatly improved in anoxic compared to oxic sediments (Rosenthal et al., 1995). For example, the average enrichment factor of Cd in Peruvian shelf sediments relative to upper continental crust is >550 (Böning et al., 2004). Resuspension of shallow shelf sediments at St. 122 may promote partial oxidation of the organically-bound Cd in the slightly oxygenated water column resulting in elevated dissolved seawater Cd contents.

4.2.1 Cd depletion in OMZ waters

The minor but significant depletion of Cd relative to PO_4 in the core of the Peruvian OMZ with O_2 < 10 μmol/kg (Fig. 5) can be attributed to authigenic sulfide precipitation within micro-environments with high organic carbon contents (e.g., Conway and John, 2015a; Janssen et al., 2014; Waeles et al., 2013). The ratio of Cd to acid-volatile sulfides on the eastern GEOTRACES GP16 transect within the Peruvian OMZ was lower than 1:1, which implies that a sulfide carrier phase may indeed be important for Cd in this region (Ohnemus et al., 2017). Detectable sulfide within large decaying organic particles has long been recognized (Shanks and Reeder 1993), and a possible role of micro CdS precipitates as an important sink for oceanic Cd was initially proposed independently for the northeast Pacific and Mauritanian OMZs (Janssen et al., 2014) and the Angola Basin (Waeles et al., 2013). These findings were later corroborated for other marine regions (Conway and John, 2015a; Conway and John, 2015b; Janssen et al., 2017; Waeles et al., 2016). A recent modeling study has further demonstrated that large (millimeter-size) decaying organic particles within the Mauritanian OMZ have the ability to host a sulfate reducing core that can provide free H_2S to bind metal cations such as Cd (Bianchi et al., 2018).

Conversely, mass balance considerations dictate that authigenic precipitation of CdS in low oxygen waters has little influence on dissolved seawater $\delta^{114/110}$Cd values. For example, the projection of data points with low Cd and O_2 contents (O_2 < 10 μmol/kg) onto the steep linear Cd-

411 PO_4 correlation of Fig. 5 suggests that ≤ 20% of Cd is lost in the Peruvian OMZ. Assuming that
412 this indeed reflects in-situ CdS precipitation and that the associated Cd isotope fractionation
413 follows a Rayleigh trend with $\alpha^{114/110}Cd_{SW\text{-}CdS}$ = 1.00029 (see discussion in session 4.2.2), this
414 would raise the $\delta^{114/110}$Cd value of the remaining dissolved Cd by only 0.06‰. This small
415 difference in $\delta^{114/110}$Cd implies that the Cd isotope compositions of OMZ waters are expected to be
416 essentially constant even if a substantial fraction of dissolved seawater Cd is removed as CdS.
417 Although authigenic CdS precipitation is likely the dominant mechanism that affects the
418 Cd-PO_4 correlation of Peruvian OMZ waters, other processes that may account for the offset of
419 some data from the linear Cd-PO_4 trend of Fig. 5 are also evaluated.
420 Firstly, it is conceivable that the depletion of Cd relative to PO_4 for the Peruvian OMZ
421 reflects addition of PO_4, for example by advection from the coast. Studies in the California and
422 Peru margins both indicate enhanced remineralization of PO_4 from reduced sediments (Ingall and
423 Jahnke, 1994; Lomnitz et al., 2015; Noffke et al., 2012) and a higher benthic flux of PO_4 can be
424 transported offshore via Ekman advection or eddy transport. However, most of the excess PO_4
425 observed for the Peruvian OMZ is confined to coastal and nearshore areas (Meyer et al., 2017),
426 and thus cannot explain the Cd-PO_4 deviations observed for the offshore stations.
427 Secondly, preferential remineralization of PO_4 relative to Cd (Xie et al., 2019) or depth-
428 dependent remineralization of suspended and sinking particulates with distinct Cd/P ratios (Wu
429 and Roshan, 2015) have been proposed to account for the Cd-PO_4 decoupling in the Mauritania
430 OMZ. These mechanisms are, however, based on Cd data for seawater with $[O_2]$ >40 μmol/kg.
431 Further studies on particulate Cd speciation are thus needed to investigate if the suggested
432 processes are also relevant for the Peruvian OMZ, where Cd-PO_4 decoupling is only observed at
433 $[O_2]$ <10 μmol/kg.
434 Lastly, changes in ecological communities may also impact the distribution of Cd and PO_4
435 in OMZs. For example, the Cd/P ratios of prokaryotes from the Peruvian OMZ were found to be
436 higher than those of the mixed layer biomass (Ohnemus et al., 2017), which may result in a slight

depletion of Cd in ambient seawater. Furthermore, a shift from autotrophic to heterotrophic biomass just above and within the upper Peruvian OMZ (Ohnemus et al., 2017) could also affect the seawater distribution of Cd, Cd isotopes and PO_4.

4.2.2 Fractionation of Cd isotopes during CdS precipitation in the presence of H_2S

A large sulfidic plume that covered an area of over 5500 km^2 on the continental shelf from 12°S to 14ºS was observed during cruise M77/3 (Schunck et al., 2013). At St. 19, H_2S concentrations of up to 4.2 µM were detected below 26 m water depth, slightly deeper than the depth at which [O_2] dropped below detection limits (Fig. S4; see supplementary material). Corresponding to the profiles of [O_2] and [H_2S], [Cd] drops from 0.46 nmol/kg at the surface to 0.05 nmol/kg at 60 m depth, whilst $\delta^{114/110}$Cd increases from 0.65‰ to 1.30‰.

The decrease in [Cd] and associated Cd isotope fractionation most likely result from in situ precipitation of dissolved Cd, with preferential incorporation of light Cd isotopes into CdS, similar to observations for low-temperature hydrothermal systems (Schmitt et al., 2009) and laboratory precipitation experiments (Guinoiseau et al., 2018). This is the first direct observation of seawater Cd isotope fractionation in a euxinic open ocean environment. As precipitation of CdS follows a Rayleigh fractionation model (Guinoiseau et al., 2018), the new data define a seawater - CdS fractionation factor of $\alpha^{114/110}Cd_{SW\text{-}CdS} = 1.00029$. Although the calculated fractionation factor is based on only two samples, it is similar to the value observed for euxinic waters of the Black Sea ($\alpha^{114/110}Cd_{SW\text{-}CdS} = 1.0003 \pm 0.0002$; Georg, 2017) and only slightly larger than that seen in CdS precipitation experiments ($\alpha^{114/110}Cd_{SW\text{-}CdS} \approx 1.00016$; Guinoiseau et al., 2018). Furthermore, using established Rayleigh fractionation equations for Cd isotopes (Abouchami et al., 2014; Ripperger et al., 2007), our data imply that the accumulated CdS precipitates are characterized by $\delta^{114/110}$Cd = -0.04‰, which agrees well with $\delta^{114/110}$Cd values of –0.18‰ to 0.16‰ reported for continental sulfides (Schmitt et al., 2009).

4.3 Cd isotopes as a water mass tracer in the eastern tropical South Pacific

Recent Cd isotope studies of the South Atlantic, the Southern Ocean, and the North and South Pacific demonstrated that Cd isotope compositions reliably trace major deep water masses (Abouchami et al., 2014; Janssen et al., 2017; Sieber et al., 2019; Xie et al., 2017; Yang et al., 2018) and a similar impact of water mass mixing on intermediate and deep water Cd isotope distributions can be shown for the ETSP.

For this evaluation, the individual samples of this study were assigned to the different water masses of the ETSP based on physical parameters (Fig. 6). The deepest samples of this study (from >3000 m) have compositions consistent with the dominant presence of PDW ([Cd] ≈ 0.93 nmol/kg; Conway and John, 2015b; Janssen et al. 2017; Yang et al., 2018) with minor admixture of less Cd-rich LCDW ([Cd] ≈ 0.75 nmol/kg; Sieber et al., 2019). This is in agreement with the water mass analysis along the GEOTRACES GP16 transect at ~12°S, which demonstrates the dominant impact of PDW (>40 %) at depths from 1200 to 4000 m for the Peruvian nearshore and offshore stations, and a shift to increasing influence of LCDW only below 3500 m depth (Peters et al., 2017). Surprisingly, a few bottom water samples from 3500 m and 4000 m at the northern stations (Sts. 109, 117, 134) show higher $\delta^{114/110}$Cd of 0.35‰ to 0.43‰ (Figs. 4 and S1). The cause of these higher $\delta^{114/110}$Cd values at depth is unclear at present, as contamination effects are unlikely for these Cd-rich waters whilst resuspension of bottom sediments should shift seawater Cd isotope compositions to lower $\delta^{114/110}$Cd (e.g. Schmitt et al., 2009).

At depths between 700 m and 3000 m, both [Cd] and $\delta^{114/110}$Cd are in accord with vertical mixing between PDW and modified AAIW, similar to that seen along the GEOTRACES GP19 section (Sieber et al., 2019). The modified AAIW identified in this study at 500 – 1100 m based on hydrographic data (Peters et al., 2017) has an average [Cd] of 0.95 nmol/kg, which exceeds the source region AAIW by nearly a factor of two (Sieber et al., 2019). However, the $\delta^{114/110}$Cd values of both modified AAIW ($\delta^{114/110}$Cd ≈ 0.49‰; this study and John et al., 2018) and AAIW from the source region ($\delta^{114/110}$Cd ≈ 0.50‰; Sieber et al., 2019) are identical within uncertainty. It thus

appears that, although aging intermediate water masses accumulate remineralized Cd en route from the Southern Ocean to the Peruvian basin, $\delta^{114/110}$Cd remains conservative.

Thus, we can constrain the Cd isotope composition of the accumulated dissolved Cd from remineralization of particulates during transport of the AAIW from the Southern Ocean to the ETSP. Using a simple mass balance and following Janssen et al. (2017), the net accumulated Cd in the ETSP is characterized by $\delta^{114/110}$Cd ≈ 0.38‰ to 0.56‰. As endmembers, this calculation uses weighted $\delta^{114/110}$Cd means of 0.50±0.05‰ (2SE; Sieber et al., 2019) for Southern Ocean AAIW and 0.49±0.01‰ for ETSP AAIW (2SE; this study and John et al., 2018). The estimated $\delta^{114/110}$Cd range for the accumulated Cd is in perfect agreement with that deduced from a steady state fractionation model with $\alpha^{114/110}Cd_{SW\text{-}biomass}$ = 1.0001 to 1.0004 (see chapter 4.1), which suggests that remineralized Cd has a similar or slightly lower $\delta^{114/110}$Cd than ETSP intermediate waters. Using a different approach and assuming Cd is completely depleted by phytoplankton uptake in the equatorial Pacific, Sieber et al. (2019) estimated a slightly larger range in $\delta^{114/110}$Cd of 0.25‰ to 0.63‰ for the remineralized Cd in the ETSP. It is noteworthy that Janssen et al. (2017) observed a similarly narrow but lower $\delta^{114/110}$Cd range of 0.13‰ to 0.42‰ for accumulated remineralized Cd in the deep subarctic North Pacific. This difference in the inferred $\delta^{114/110}$Cd of accumulated dissolved Cd may result from distinct water mass compositions or differences in nutrient supply to the surface ocean and local biological uptake intensities.

5. Conclusions

Cadmium concentrations and isotope compositions are reported for the water column of the ETSP from 12 coastal, nearshore and offshore stations between 4ºS and 14ºS. The data reveal several distinct aspects of the marine biogeochemical cycling of Cd and Cd isotopes that are important for low oxygen environments.

The surface waters have highly variable Cd concentrations but a nearly constant Cd isotope signature. This observation is consistent with a steady-state fractionation model for the biological

uptake of Cd from surface waters. In contrast, the diverse Cd isotope systematics of intermediate depth water masses are best explained by mixing of remineralized Cd with ambient seawater.

Small but significant deviations from the regional seawater Cd-PO_4 correlation towards lower Cd concentration are observed for all stations with O_2 < 10 μmol/kg. This decoupling is attributed to in situ CdS precipitation in microenvironments with millimeter-scale decaying organic matter, in accord with the conclusions of previous studies. A large H_2S plume was detected at a single coastal station resulting in significantly depleted [Cd] and heavier Cd isotope compositions, in accord with an isotope fractionation factor of $\alpha^{114/110}Cd_{SW\text{-}CdS} = 1.00029$.

These results suggest that further deoxygenation in the future global ocean may have two key impacts on the biogeochemistry of Cd in subsurface waters. First, climatically forced changes in global ocean oxygen concentrations are expected to reduce (increase) particle-related denitrification at low (high) latitudes in the Pacific Ocean (Bianchi et al., 2018). As both particle-related denitrification and CdS precipitation occur within decaying organic matter in the presence of dissolved O_2 in ambient seawater (Bianchi et al., 2018; and references therein), similar impacts of climate are hence expected for both processes. Second, increasing deoxygenation may promote bottom water hypoxia and H_2S events along the shallow continental shelf off Peru (Lavik et al., 2009; Schlosser et al., 2018). This will likely result in more frequent occurrences of bottom water Cd depletion, whereby isotopically light Cd is stored in sediments as CdS.

The deep ocean distribution of $\delta^{114/110}Cd$ in the ETSP appears to be governed by water mass mixing, similar to that observed for the Atlantic, Southern, and western and South Pacific Oceans. However, the modified AAIW of the ETSP is characterized by a two-fold higher [Cd] than AAIW at its source region, whilst both water masses have similar $\delta^{114/110}Cd$. These observations constrain that the accumulated remineralized Cd in the ETSP has a $\delta^{114/110}Cd$ of between 0.38‰ and 0.56‰, in perfect agreement with the steady state model calculation.

Acknowledgements

We thank Lothar Stramma, the scientific party and the crews on board of cruises METEOR M77/3 and M77/4 for their help in sample collection. These cruises were part of the German Collaborative Research Centre (SFB) 754: Climate – Biogeochemistry Interactions in the Tropical Ocean funded by the German Science Foundation. Barry J Coles, Katharina Kreissig, Rasmus Andreasen, Roz Coggon and other members of the MAGIC team are thanked for their help and laboratory support. This research was made possible by funding from NERC research grants NE/G008973/1 and NE/H005390/1 to MR and an Imperial College Lee Family Scholarship to ZX. RCX and PG were funded by the SFB 754.

550 **References**
551
552 Abe, K., 2002. Preformed Cd and PO_4 and the relationship between the two elements in the
553 northwestern Pacific and the Okhotsk Sea. Marine Chemistry 79, 27-36.
554 Abouchami, W., Galer, S.J.G., de Baar, H.J.W., Alderkamp, A.C., Middag, R., Laan, P.,
555 Feldmann, H., Andreae, M.O., 2011. Modulation of the Southern Ocean cadmium isotope
556 signature by ocean circulation and primary productivity. Earth and Planetary Science
557 Letters 305, 83-91.
558 Abouchami, W., Galer, S.J.G., de Baar, H.J.W., Middag, R., Vance, D., Zhao, Y., Klunder, M.,
559 Mezger, K., Feldmann, H., Andreae, M.O., 2014. Biogeochemical cycling of cadmium
560 isotopes in the Southern Ocean along the Zero Meridian. Geochimica et Cosmochimica
561 Acta 127, 348-367.
562 Abouchami, W., Galer, S.J.G., Horner, T.J., Rehkämper, M., Wombacher, F., Xue, Z., Lambelet,
563 M., Gault‐Ringold, M., Stirling, C.H., Schönbächler, M., 2013. A common reference
564 material for cadmium isotope studies‐NIST SRM 3108. Geostandards and Geoanalytical
565 Research 37, 5-17.
566 Baars, O., Abouchami, W., Galer, S.J.G., Boye, M., Croot, P.L., 2014. Dissolved cadmium in the
567 Southern Ocean: Distribution, speciation, and relation to phosphate. Limnology and
568 Oceanography 59, 385-399.
569 Bianchi, D., Weber, T.S., Kiko, R., Deutsch, C., 2018. Global niche of marine anaerobic
570 metabolisms expanded by particle microenvironments. Nature Geoscience 11, 263.
571 Böning, P., Brumsack, H.-J., Böttcher, M.E., Schnetger, B., Kriete, C., Kallmeyer, J., Borchers,
572 S.L., 2004. Geochemistry of Peruvian near-surface sediments. Geochimica et
573 Cosmochimica Acta 68, 4429-4451.
574 Boyle, E.A., 1988. Cadmium: Chemical tracer of deepwater paleoceanography. Paleoceanography
575 3, 471-489.

576 Boyle, E.A., Sclater, F., Edmond, J.M., 1976. On the marine geochemistry of cadmium. Nature
577 263, 42-44.
578 Bruland, K.W., Knauer, G.A., Martin, J.H., 1978. Cadmium in northeast Pacific waters.
579 Limnology and Oceanography 23, 618-625.
580 Bruland, K.W., Rue, E.L., Smith, G.J., DiTullio, G.R., 2005. Iron, macronutrients and diatom
581 blooms in the Peru upwelling regime: brown and blue waters of Peru. Marine Chemistry
582 93, 81-103.
583 Cantrell, C., 2008. Review of methods for linear least-squares fitting of data and application to
584 atmospheric chemistry problems. Atmospheric Chemistry and Physics 8, 5477-5487.
585 Conway, T.M., John, S.G., 2015a. Biogeochemical cycling of cadmium isotopes along a high-
586 resolution section through the North Atlantic Ocean. Geochimica et Cosmochimica Acta
587 148, 269-283.
588 Conway, T.M., John, S.G., 2015b. The cycling of iron, zinc and cadmium in the North East Pacific
589 Ocean – Insights from stable isotopes. Geochimica et Cosmochimica Acta 164, 262-283.
590 Cullen, J.T., 2006. On the nonlinear relationship between dissolved cadmium and phosphate in the
591 modern global ocean: Could chronic iron limitation of phytoplankton growth cause the
592 kink? Limnology and Oceanography 51, 1369-1380.
593 de Baar, H.J.W., Saager, P.M., Nolting, R.F., van der Meer, J., 1994. Cadmium versus phosphate
594 in the world ocean. Marine Chemistry 46, 261-281.
595 Fiedler, P.C., Talley, L.D., 2006. Hydrography of the eastern tropical Pacific: A review. Progress
596 in Oceanography 69, 143-180.
597 Frew, R.D., Hunter, K.A., 1992. Influence of Southern Ocean waters on the cadmium-phosphate
598 properties of the global ocean. Nature 360, 144-146.
599 Frew, R.D., Hunter, K.A., 1995. Cadmium-phosphorus cycling at the subtropical convergence
600 south of New Zealand. Marine Chemistry 51, 223-237.

Gault-Ringold, M., Adu, T., Stirling, C.H., Frew, R.D., Hunter, K.A., 2012. Anomalous biogeochemical behavior of cadmium in subantarctic surface waters: Mechanistic constraints from cadmium isotopes. Earth and Planetary Science Letters 341–344, 94-103.

Georg, E., 2017. Marine biogeochemical cycling of cadmium and its isotopes: Studies of the South Pacific Ocean, Mediterranean Sea and Black Sea, Chemistry. University of Otago, Otago university Research Archive.

Grasse, P., Ehlert, C., Frank, M., 2013. The influence of water mass mixing on the dissolved Si isotope composition in the Eastern Equatorial Pacific. Earth and Planetary Science Letters 380, 60-71.

Grasse, P., Ryabenko, E., Ehlert, C., Altabet, M.A., Frank, M., 2016. Silicon and nitrogen cycling in the upwelling area off Peru: A dual isotope approach. Limnology and Oceanography 61, 1661-1676.

Guinoiseau, D., Galer, S.J. and Abouchami, W., 2018. Effect of cadmium sulphide precipitation on the partitioning of Cd isotopes: Implications for the oceanic Cd cycle. Earth and Planetary Science Letters, 498, pp.300-308.

Henson, S.A., Sanders, R., Madsen, E., 2012. Global patterns in efficiency of particulate organic carbon export and transfer to the deep ocean. Global Biogeochemical Cycles 26, n/a-n/a.

Huyer, A., Smith, R.L., Paluszkiewicz, T., 1987. Coastal upwelling off Peru during normal and El Niño times, 1981–1984. Journal of Geophysical Research: Oceans 92, 14297-14307.

Ingall, E., Jahnke, R., 1994. Evidence for enhanced phosphorus regeneration from marine sediments overlain by oxygen depleted waters. Geochimica et Cosmochimica Acta 58, 2571-2575.

Janssen, D.J., Abouchami, W., Galer, S.J.G., Cullen, J.T., 2017. Fine-scale spatial and interannual cadmium isotope variability in the subarctic northeast Pacific. Earth and Planetary Science Letters 472, 241-252.

626 Janssen, D.J., Conway, T.M., John, S.G., Christian, J.R., Kramer, D.I., Pedersen, T.F., Cullen,
627 J.T., 2014. Undocumented water column sink for cadmium in open ocean oxygen-deficient
628 zones. Proceedings of the National Academy of Sciences 111, 6888-6893.
629 John, S.G., Conway, T.M., 2014. A role for scavenging in the marine biogeochemical cycling of
630 zinc and zinc isotopes. Earth and Planetary Science Letters 394, 159-167.
631 John, S.G., Helgoe, J., Townsend, E., 2018. Biogeochemical cycling of Zn and Cd and their stable
632 isotopes in the Eastern Tropical South Pacific. Marine Chemistry 201, 256-262.
633 Karstensen, J., 2004. Formation of the South Pacific shallow salinity minimum: A Southern Ocean
634 pathway to the tropical Pacific. Journal of physical oceanography 34, 2398-2412.
635 Kawabe, M., Fujio, S., 2010. Pacific Ocean circulation based on observation. Journal of
636 oceanography 66, 389.
637 Lacan, F., Francois, R., Ji, Y., Sherrell, R.M., 2006. Cadmium isotopic composition in the ocean.
638 Geochimica et Cosmochimica Acta 70, 5104-5118.
639 Lane, T.W., Morel, F.M., 2000. A biological function for cadmium in marine diatoms.
640 Proceedings of the National Academy of Sciences 97, 4627-4631.
641 Lavik, G., Stührmann, T., Brüchert, V., Van der Plas, A., Mohrholz, V., Lam, P., Mußmann, M.,
642 Fuchs, B.M., Amann, R., Lass, U., 2009. Detoxification of sulphidic African shelf waters
643 by blooming chemolithotrophs. Nature 457, 581.
644 Llanillo, P., Karstensen, J., Pelegrí, J., Stramma, L., 2013. Physical and biogeochemical forcing of
645 oxygen and nitrate changes during El Niño/El Viejo and La Niña/La Vieja upper-ocean
646 phases in the tropical eastern South Pacific along 86° W. Biogeosciences (BG) 10, 6339-
647 6355.
648 Lomnitz, U., Sommer, S., Dale, A., Löscher, C., Noffke, A., Wallmann, K., Hensen, C., 2015.
649 Benthic phosphorus cycling in the Peruvian oxygen minimum zone. Biogeosciences
650 Discussions 12.

651 Meyer, J., Löscher, C.R., Lavik, G., Riebesell, U., 2017. Mechanisms of P* Reduction in the
652 Eastern Tropical South Pacific. Frontiers in Marine Science 4.
653 Noffke, A., Hensen, C., Sommer, S., Scholz, F., Bohlen, L., Mosch, T., Graco, M., Wallmann, K.,
654 2012. Benthic iron and phosphorus fluxes across the Peruvian oxygen minimum zone.
655 Limnology and Oceanography 57, 851-867.
656 Ohnemus, D.C., Rauschenberg, S., Cutter, G.A., Fitzsimmons, J.N., Sherrell, R.M., Twining, B.S.,
657 2017. Elevated trace metal content of prokaryotic communities associated with marine
658 oxygen deficient zones. Limnology and Oceanography 62, 3-25.
659 Penven, P., Echevin, V., Pasapera, J., Colas, F., Tam, J., 2005. Average circulation, seasonal cycle,
660 and mesoscale dynamics of the Peru Current System: A modeling approach. Journal of
661 Geophysical Research: Oceans (1978–2012) 110.
662 Peters, B.D., Jenkins, W.J., Swift, J.H., German, C.R., Moffett, J.W., Cutter, G.A., Brzezinski,
663 M.A., Casciotti, K.L., 2017. Water mass analysis of the 2013 US GEOTRACES eastern
664 Pacific zonal transect (GP16). Marine Chemistry.
665 Price, N., Morel, F., 1990. Cadmium and cobalt substitution for zinc in a marine diatom. Nature
666 344, 658-660.
667 Reid, J.L., 1973. The shallow salinity minima of the Pacific Ocean, Deep Sea Research and
668 Oceanographic Abstracts. Elsevier, pp. 51-68.
669 Ripperger, S., Rehkämper, M., 2007. Precise determination of cadmium isotope fractionation in
670 seawater by double spike MC-ICPMS. Geochimica et Cosmochimica Acta 71, 631-642.
671 Ripperger, S., Rehkämper, M., Porcelli, D., Halliday, A., 2007. Cadmium isotope fractionation in
672 seawater—A signature of biological activity. Earth and Planetary Science Letters 261, 670-
673 684.
674 Schmitt, A.-D., Galer, S.J.G., Abouchami, W., 2009. Mass-dependent cadmium isotopic variations
675 in nature with emphasis on the marine environment. Earth and Planetary Science Letters
676 277, 262-272.

677 Shanks, A.L., Reeder, M.L., 1993. Reducing microzones and sulfide production in marine snow.
678 Marine Ecology Progress Series 96, 43-47.
679 Sieber, M., Conway, T., de Souza, G., Obata, H., Takano, S., Sohrin, Y., Vance, D., 2019.
680 Physical and biogeochemical controls on the distribution of dissolved cadmium and its
681 isotopes in the Southwest Pacific Ocean. Chemical Geology, in press,
682 doi.org/10.1016/j.chemgeo.2018.07.021.
683 Schlosser, C., Streu, P., Frank, M., Lavik, G., Croot, P.L., Dengler, M., Achterberg, E.P., 2018.
684 H_2S events in the Peruvian oxygen minimum zone facilitate enhanced dissolved Fe
685 concentrations. Scientific Reports 8, 12642.
686 Schunck, H., Lavik, G., Desai, D.K., Großkopf, T., Kalvelage, T., Löscher, C.R., Paulmier, A.,
687 Contreras, S., Siegel, H., Holtappels, M., 2013. Giant hydrogen sulfide plume in the
688 oxygen minimum zone off Peru supports chemolithoautotrophy. PLoS One 8, e68661.
689 Silva, N., Rojas, N., Fedele, A., 2009. Water masses in the Humboldt Current System: Properties,
690 distribution, and the nitrate deficit as a chemical water mass tracer for Equatorial
691 Subsurface Water off Chile. Deep Sea Research Part II: Topical Studies in Oceanography
692 56, 1004-1020.
693 Tsuchiya, M., Talley, L.D., 1998. A Pacific hydrographic section at 88 W: Water‐property
694 distribution. Journal of Geophysical Research: Oceans 103, 12899-12918.
695 Waeles, M., Maguer, J.-F., Baurand, F., Riso, R.D., 2013. Off Congo waters (Angola Basin,
696 Atlantic Ocean): A hot spot for cadmium-phosphate fractionation. Limnology and
697 Oceanography 58, 1481-1490.
698 Waeles, M., Planquette, H., Afandi, I., Delebecque, N., Bouthir, F., Donval, A., Shelley, R.U.,
699 Auger, P.A., Riso, R.D., Tito de Morais, L., 2016. Cadmium in the waters off South
700 Morocco: Nature of particles hosting Cd and insights into the mechanisms fractionating Cd
701 from phosphate. Journal of Geophysical Research: Oceans 121, 3106-3120.

Wu, J., Roshan, S., 2015. Cadmium in the North Atlantic: Implication for global cadmium–phosphorus relationship. Deep Sea Research Part II: Topical Studies in Oceanography 116, 226-239.

Xie, R.C., Galer, S.J., Abouchami, W., Rijkenberg, M.J., de Baar, H.J., De Jong, J., Andreae, M.O., 2017. Non-Rayleigh control of upper-ocean Cd isotope fractionation in the western South Atlantic. Earth and Planetary Science Letters 471, 94-103.

Xie, R.C., Galer, S.J.G., Abouchami, W., Frank, M., 2019. Limited impact of eolian and riverine sources to the biogeochemical cycling of Cd in the Tropical Atlantic. Chemical Geology, in press, doi.org/10.1016/j.chemgeo.2018.10.018.

Xie, R.C., Galer, S.J.G., Abouchami, W., Rijkenberg, M.J.A., De Jong, J., de Baar, H.J.W., Andreae, M.O., 2015. The cadmium–phosphate relationship in the western South Atlantic - The importance of mode and intermediate waters on the global systematics. Marine Chemistry 177, Part 1, 110-123.

Xue, Z., Rehkämper, M., Horner, T.J., Abouchami, W., Middag, R., van de Flierdt, T., de Baar, H.J.W., 2013. Cadmium isotope variations in the Southern Ocean. Earth and Planetary Science Letters 382, 161-172.

Xue, Z., Rehkämper, M., Schönbächler, M., Statham, P., Coles, B., 2012. A new methodology for precise cadmium isotope analyses of seawater. Anal Bioanal Chem 402, 883-893.

Yang, J., Li, Y., Liu, S., Tian, H., Chen, C., Liu, J., Shi, Y., 2015. Theoretical calculations of Cd isotope fractionation in hydrothermal fluids. Chemical Geology 391, 74-82.

Yang, S.-C., Zhang, J., Sohrin, Y., Ho, T.-Y., 2018. Cadmium cycling in the water column of the Kuroshio-Oyashio Extension region: Insights from dissolved and particulate isotopic composition. Geochimica et Cosmochimica Acta 233, 66-80.

728 **Figure captions**

729 Figure 1: (a) Sampling locations off Peru occupied during R/V Meteor cruises M77-3 and M77-4
730 in January and February 2009. Profiles are divided into three groups according to their distance
731 from land. 'Offshore' stations along 85'50°W (Sts. 109, 134, 97, 93) and St. 86 are marked in blue
732 colors. 'Nearshore' stations (Sts. 117, 124, 11, 78) are marked in yellow and red colors whilst
733 'coastal' stations are shown in green colors. (b) Sea surface temperatures (SSTs; °C) obtained
734 during M77-3 and M77-4 with a schematic overview of important surface and subsurface currents
735 according to Montes et al. (2010) and Czeschel et al. (2011). Solid lines indicate surface currents
736 and dashed lines show subsurface currents. PCC: Peru Coastal Current; EUC: Equatorial
737 Undercurrent (~100 m); SSCC: Southern Subsurface Countercurrent (~50 m to 750 m); SECC:
738 South Equatorial Countercurrent (~50 m to 300 m); PCUC: Peru-Chile Undercurrent; POC: Peru
739 Oceanic Current (also called Humboldt Current, HC; surface to 750 m). Data were plotted using
740 ODV 4.6.2 (Schlitzer, 2014).

741

742

743 Figure 2: T-S diagram with potential density (σ_θ) for all stations of this study. Colors indicate the
744 dissolved oxygen concentration (µmol/kg) at the corresponding depths. Note the inset figure for
745 the intermediate and deep ocean (> 26.5 kg/m^3). Surface (≤ 25 kg/m^3), subsurface (25 to 26.5
746 kg/m^3), intermediate (26.5 to 27.5 kg/m^3) and deep water masses (> 27.5 kg/m^3) are defined
747 according to Schneider et al. (2003); Karstensen et al. (2004); Fiedler and Talley (2006) and Silva
748 et al. (2009). STSW: Subtropical Surface Water; ESW: Equatorial surface Water; TSW: Tropical
749 Surface Water; SSMW: Shallow Salinity Minimum (also called Eastern South Pacific Intermediate
750 Water, ESPIW); ESSW: Equatorial Subsurface Water; AAIW: Antarctic Intermediate Water;
751 EqPIW: Equatorial Pacific Intermediate Water; PDW: Pacific Deep Water.

752

753 Figure 3. Depth profiles of the upper 1500 m (upper 160 m for coastal stations) for $\delta^{114/110}Cd$ (blue
754 circles) and the concentrations of Cd (red circles), oxygen (green), and PO_4 (grey circles) for the
755 offshore (left), nearshore (middle), and coastal (right) stations.
756
757 Figure 4. Cd isotope systematics colored coded with (a) oxygen concentrations and (b) potential
758 density. Gray and black lines in (a) highlight the isotopic evolution of seawater for steady state
759 isotope fractionation with $\alpha^{114/110}Cd_{SW\text{-}biomass}$ = 1.0001 and 1.0004, using starting compositions of
760 [Cd] = 0.71 nmol/kg, $\delta^{114/110}Cd$ = 0.57‰ (dashed lines), and [Cd] = 0.63 nmol/kg, $\delta^{114/110}Cd$ =
761 0.54‰ (solid lines). Cyan and blue lines in (b) are mixing curves between seawater and
762 remineralized Cd, with biomass $\delta^{114/110}Cd$ of 0.17‰ and 0.51‰ and seawater compositions of
763 [Cd] = 0.43, $\delta^{114/110}Cd$ = 0.66‰ (solid lines), and [Cd] = 0.58 nmol/kg, $\delta^{114/110}Cd$ = 0.80‰
764 (dashed lines); see supplementary material for details.
765
766 Figure 5. Cross plot of dissolved Cd and PO_4 for the eastern South Pacific OMZ. (Left) Station
767 color coding is the same as in Figure 1. In the right panel, Samples are subdivided into those from
768 the surface (grey circles), and those above (purple), within (blue circles) and below (orange
769 circles) the core of the OMZ. Blue arrows highlight the deviation of low-oxygen waters from the
770 linear Cd-PO_4 correlation. Grey and black dashed lines are the Williamson-York bivariate fits
771 (Cantrell, 2008) of the surface and deep (excluding St. 19 and 122, and OMZ samples) waters,
772 respectively. The dotted grey line shows the linear trend defined by data for the eastern Pacific
773 GP16 section of the GEOTRACES programme (John et al., 2018).
774
775 Figure 6. Cross plot of $\delta^{114/110}Cd$ *vs.* 1/[Cd], illustrating the influence of water mass mixing on the
776 biogeochemistry of Cd isotopes in the deep ETSP. Colors representing the major water masses are
777 assigned to the samples. Colored boxes indicate endmember values for the water mass source
778 regions. The inset displays the data for all samples. Note the difference in [Cd] between the

779 modified AAIW of the ESTP and the AAIW from the Southern Ocean source region. Water mass
780 acronyms are: ESW – Equatorial Surface Water; STSW – Subtropical Surface Water; SSMW –
781 Shallow Salinity Minimum Water; ESSW – Equatorial Subsurface Water; AAIW – Antarctic
782 Intermediate Water; EqPIW – Equatorial Pacific Intermediate Water; PDW – Pacific Deep Water;
783 LCDW – Lower Circumpolar Deep Water.

Table 1. Cd concentrations and isotope compositions, along with physical parameters and macronutrient concentrations for seawater samples analyzed in this study. $\varepsilon^{114/110}$Cd values are reported relatively to NIST SRM3108 standard and converted to $\delta^{114/110}$Cd for interlaboratory comparison.

Cruise	Station	Transect	Cast	Latitude	Longitude	Depth	Potential Density	Temperature	Salinity	O_2 (CTD)	Chl a	NO_3	NO_2	PO_4	Cd	$\varepsilon^{114/110}$Cd	2σ	$\delta^{114/110}$Cd	2σ
						m	kg/m3	°C	PSS-78	µmol/kg		µmol/kg	µmol/kg	µmol/kg	nmol/kg			‰	
M77-3	11	Nearshore	35	-12.03	-78.00	2	24.44	21.2	34.99	255.1	1.16	0.63	0.19	1.10	0.12	8.1	0.4	0.81	0.04
M77-3	11	Nearshore	35	-12.03	-78.00	50	26.13	14.2	34.98	2.8	0.06	30.00	0.29	2.65	0.77	7.2	0.5	0.72	0.05
M77-3	11	Nearshore	35	-12.03	-78.00	99	26.32	13.2	34.95	1.9	0.06	20.90	4.91	2.88	0.74	5.7	0.4	0.57	0.04
M77-3	11	Nearshore	35	-12.03	-78.00	199	26.46	12.3	34.89	2.1	0.06	28.24	2.84	2.78	0.71	5.8	0.6	0.58	0.06
M77-3	11	Nearshore	35	-12.03	-78.00	694	27.23	5.8	34.54	20.2	0.05	51.30	0.10	3.50	1.06	4.8	0.5	0.48	0.05
M77-3	11	Nearshore	35	-12.03	-78.00	1485	27.59	3.0	34.61	76.5	0.05	44.87	0.13	3.23	1.01	3.4	0.6	0.34	0.06
M77-3	19	Coastal	50	-12.36	-77.00	7	25.95	15.1	34.99	17.2	0.32	-	-	-	0.46	6.5	0.8	0.65	0.08
M77-3	19	Coastal	50	-12.36	-77.00	60	26.22	13.8	34.97	2.0	0.17	-	-	-	0.05	13.1	2.3	1.31	0.23
M77-4	78	Nearshore	4	-14.00	-77.06	2	24.77	19.8	34.93	222.2	1.07	-	-	-	0.31	8.2	0.5	0.82	0.05
M77-4	78	Nearshore	4	-14.00	-77.06	21	25.71	15.9	34.92	128.7	0.21	-	-	-	0.54	8.7	0.5	0.87	0.05
M77-4	78	Nearshore	4	-14.00	-77.06	49	26.07	14.5	34.97	2.8	0.08	-	-	-	0.84	7.7	0.5	0.77	0.05
M77-4	78	Nearshore	4	-14.00	-77.06	100	26.26	13.5	34.95	2.8	0.07	-	-	-	0.75	6.3	0.4	0.63	0.04
M77-4	78	Nearshore	4	-14.00	-77.06	199	26.44	12.4	34.89	3.0	0.06	-	-	-	0.71	5.5	0.4	0.55	0.04
M77-4	78	Nearshore	4	-14.00	-77.06	397	26.85	9.2	34.67	3.2	0.06	-	-	-	0.87	5.4	0.6	0.54	0.06
M77-4	78	Nearshore	4	-14.00	-77.06	904	27.33	4.9	34.53	40.7	0.05	-	-	-	1.07	4.7	0.5	0.47	0.05
M77-4	78	Nearshore	3	-14.00	-77.06	1485	27.59	3.0	34.60	82.7	0.05	-	-	-	1.02	3.9	0.6	0.39	0.06
M77-4	78	Nearshore	3	-14.00	-77.06	2986	27.76	1.8	34.68	132.6	0.04	-	-	-	0.89	2.7	0.6	0.27	0.06
M77-4	86	Offshore	12	-14.00	-82.00	3	23.62	24.6	35.21	215.5	0.08	-	-	-	0.03	5.6	2.0	0.56	0.20
M77-4	86	Offshore	12	-14.00	-82.00	26	25.13	19.0	35.12	252.9	0.21	-	-	-	0.04	4.2	2.6	0.42	0.26
M77-4	86	Offshore	12	-14.00	-82.00	72	25.61	16.2	34.88	195.5	0.11	-	-	-	0.24	6.8	0.8	0.68	0.08
M77-4	86	Offshore	12	-14.00	-82.00	109	26.14	14.0	34.92	9.1	0.06	-	-	-	0.79	6.2	0.6	0.62	0.06
M77-4	86	Offshore	12	-14.00	-82.00	198	26.44	12.2	34.86	3.0	0.06	-	-	-	0.68	6.1	0.4	0.61	0.04
M77-4	86	Offshore	12	-14.00	-82.00	397	26.84	9.2	34.67	7.7	0.05	-	-	-	0.81	5.8	0.4	0.58	0.04
M77-4	86	Offshore	12	-14.00	-82.00	792	27.24	5.5	34.51	35.1	0.05	-	-	-	1.04	4.8	1.0	0.48	0.10
M77-4	93	Offshore	19	-14.00	-85.83	3	23.82	24.7	35.52	221.2	0.38	3.72	0.08	0.53	0.02	6.5	1.9	0.65	0.19
M77-4	93	Offshore	19	-14.00	-85.83	26	23.95	24.1	35.45	223.2	0.45	4.79	0.14	0.62	0.02	7.2	2.6	0.72	0.26
M77-4	93	Offshore	19	-14.00	-85.83	149	26.22	13.3	34.83	18.3	0.05	21.15	0.18	2.68	0.70	6.9	0.4	0.69	0.04
M77-4	93	Offshore	19	-14.00	-85.83	199	26.44	12.1	34.83	3.0	0.05	20.86	1.72	2.73	0.65	5.9	0.5	0.59	0.05
M77-4	93	Offshore	19	-14.00	-85.83	348	26.79	9.6	34.69	4.4	0.05	35.42	0.00	2.87	0.80	5.7	0.4	0.57	0.04
M77-4	93	Offshore	18	-14.00	-85.83	794	27.29	5.2	34.53	38.0	0.05	45.76	0.01	3.26	1.03	4.0	0.7	0.40	0.07
M77-4	93	Offshore	18	-14.00	-85.83	1487	27.57	3.0	34.59	86.6	0.05	41.03	0.00	3.02	0.99	3.2	1.1	0.32	0.11
M77-4	93	Offshore	18	-14.00	-85.83	2964	27.76	1.8	34.68	132.4	0.04	37.58	0.01	2.66	0.88	2.3	0.7	0.23	0.07
M77-4	93	Offshore	18	-14.00	-85.83	3976	27.78	1.8	34.69	153.0	0.04	35.71	0.02	2.53	0.83	2.7	0.7	0.27	0.07
M77-4	97	Offshore	23	-12.00	-85.83	2	23.80	24.9	35.56	218.8	0.13	4.05	0.09	0.54	0.01	4.7	2.3	0.47	0.23
M77-4	97	Offshore	23	-12.00	-85.83	51	25.32	18.7	35.28	229.8	0.34	2.81	0.21	0.73	0.04	7.9	2.0	0.79	0.20
M77-4	97	Offshore	23	-12.00	-85.83	149	26.26	13.0	34.81	6.3	0.05	21.35	0.02	2.66	0.67	6.9	0.4	0.69	0.04
M77-4	97	Offshore	23	-12.00	-85.83	248	26.60	11.1	34.79	6.3	0.05	31.09	0.00	2.67	0.65	5.6	0.5	0.56	0.05
M77-4	97	Offshore	23	-12.00	-85.83	499	27.02	7.6	34.58	20.9	0.05	40.83	0.00	3.06	0.92	5.2	0.8	0.52	0.08
M77-4	97	Offshore	23	-12.00	-85.83	991	27.39	4.5	34.55	54.1	0.05	43.29	0.01	3.19	1.02	3.9	0.9	0.39	0.09
M77-4	109	Offshore	35	-3.58	-85.83	2	22.81	25.5	34.49	215.0	0.25	6.33	0.19	0.59	0.04	6.8	1.4	0.68	0.14
M77-4	109	Offshore	35	-3.58	-85.83	51	25.98	15.3	35.08	69.2	0.25	24.00	0.85	1.74	0.53	7.5	0.5	0.75	0.05
M77-4	109	Offshore	35	-3.58	-85.83	150	26.26	13.5	34.96	46.4	0.04	27.64	0.01	2.00	0.55	4.9	0.4	0.49	0.04
M77-4	109	Offshore	35	-3.58	-85.83	247	26.39	12.8	34.92	4.6	0.05	31.91	0.00	2.44	0.70	5.4	0.7	0.54	0.07
M77-4	109	Offshore	35	-3.58	-85.83	438	26.90	8.8	34.67	11.0	0.05	38.47	0.01	2.87	0.84	5.2	0.5	0.52	0.05
M77-4	109	Offshore	35	-3.58	-85.83	696	27.19	6.3	34.57	22.0	0.05	42.80	0.00	3.08	0.99	4.4	0.8	0.44	0.08

M77-4	109	Offshore	35	-3.58	-85.83	1487	27.57	3.2	34.61	80.0	0.05	40.83	0.00	3.02	0.95	3.6	0.6	0.36	0.06
M77-4	109	Offshore	35	-3.58	-85.83	3160	27.76	1.8	34.68	134.1	0.04	37.09	0.01	2.67	0.88	3.5	0.9	0.35	0.09
M77-4	117	Nearshore	45	-3.58	-82.02	2	23.66	22.5	34.46	195.2	0.14	7.67	0.21	0.74	0.10	6.8	0.5	0.68	0.05
M77-4	117	Nearshore	45	-3.58	-82.02	31	25.94	15.6	35.11	77.0	0.25	21.84	0.67	1.62	0.43	6.6	0.4	0.66	0.04
M77-4	117	Nearshore	45	-3.58	-82.02	150	26.24	13.6	34.96	47.0	0.04	26.95	0.01	1.97	0.54	5.4	0.4	0.54	0.04
M77-4	117	Nearshore	45	-3.58	-82.02	346	26.74	10.3	34.77	3.3	0.06	33.94	0.24	2.81	0.80	4.8	0.4	0.48	0.04
M77-4	117	Nearshore	44	-3.58	-82.02	794	27.25	5.9	34.58	43.9	0.05	41.23	0.01	3.00	0.93	4.7	0.4	0.47	0.04
M77-4	117	Nearshore	44	-3.58	-82.02	1487	27.57	3.2	34.61	79.1	0.05	40.64	0.00	2.99	0.96	3.7	0.4	0.37	0.04
M77-4	117	Nearshore	44	-3.58	-82.02	2963	27.76	1.8	34.68	130.2	0.04	36.70	0.01	2.66	0.88	3.7	0.4	0.37	0.04
M77-4	120	Nearshore	48	-3.59	-80.95	21	24.16	20.2	34.26	185.6	1.17	15.65	0.21	1.37	0.19	7.4	0.6	0.74	0.06
M77-4	120	Nearshore	48	-3.59	-80.95	150	26.14	14.2	34.98	47.2	0.05	25.88	0.00	1.96	0.53	3.4	0.6	0.34	0.06
M77-4	122	Coastal	50	-6.00	-81.26	6	25.44	17.3	35.00	113.9	0.85	20.75	0.56	1.82	0.63	7.2	0.5	0.72	0.05
M77-4	122	Coastal	50	-6.00	-81.26	11	25.80	15.8	35.01	46.2	0.67	27.84	0.35	2.13	0.84	6.1	0.6	0.61	0.06
M77-4	122	Coastal	50	-6.00	-81.26	51	26.06	14.7	35.02	7.4	0.07	30.30	0.02	2.22	0.83	5.3	0.5	0.53	0.05
M77-4	122	Coastal	50	-6.00	-81.26	99	26.15	14.2	34.99	4.3	0.05	30.39	0.01	2.33	0.94	6.1	0.4	0.61	0.04
M77-4	124	Nearshore	53	-6.00	-81.75	2	24.23	21.9	34.97	205.4	0.78	10.13	0.36	1.00	0.11	8.1	0.5	0.81	0.05
M77-4	124	Nearshore	53	-6.00	-81.75	12	25.29	18.2	35.07	82.4	0.38	20.46	0.46	1.73	0.58	8.0	0.4	0.80	0.04
M77-4	124	Nearshore	53	-6.00	-81.75	41	26.09	14.5	35.01	12.6	0.07	30.05	0.08	2.19	0.72	5.4	0.4	0.54	0.04
M77-4	124	Nearshore	53	-6.00	-81.75	201	26.32	13.2	34.94	3.7	0.05	31.28	0.01	2.42	0.73	5.0	0.5	0.50	0.05
M77-4	124	Nearshore	52	-6.00	-81.75	795	27.24	5.8	34.56	30.3	0.05	44.28	0.00	3.17	0.99	4.1	0.5	0.41	0.05
M77-4	124	Nearshore	52	-6.00	-81.75	1486	27.58	3.1	34.61	79.0	0.05	41.52	0.01	3.03	0.97	4.3	0.5	0.43	0.05
M77-4	124	Nearshore	52	-6.00	-81.75	2963	27.76	1.8	34.68	127.8	0.04	37.58	0.01	2.70	0.89	2.9	0.3	0.29	0.03
M77-4	124	Nearshore	52	-6.00	-81.75	3942	27.77	1.8	34.68	138.0	0.04	36.40	0.02	2.62	0.87	2.5	0.3	0.25	0.03
M77-4	134	Nearshore	64	-6.00	-85.83	2	22.29	26.9	34.39	218.8	0.20	4.18	0.11	0.39	0.04	5.5	0.6	0.55	0.06
M77-4	134	Nearshore	64	-6.00	-85.83	24	24.15	22.5	35.09	202.9	0.46	10.52	0.36	0.96	0.13	6.5	0.4	0.65	0.04
M77-4	134	Nearshore	64	-6.00	-85.83	75	26.15	14.3	35.01	18.2	0.08	29.31	0.06	2.12	0.70	6.6	0.6	0.66	0.06
M77-4	134	Nearshore	64	-6.00	-85.83	89	26.18	14.0	34.99	30.7	0.06	29.41	0.06	2.16	0.65	5.8	0.6	0.58	0.06
M77-4	134	Nearshore	64	-6.00	-85.83	247	26.45	12.4	34.91	11.2	0.05	32.36	0.00	2.39	0.69	4.8	0.6	0.48	0.06
M77-4	134	Nearshore	64	-6.00	-85.83	397	26.83	9.5	34.71	3.2	0.06	32.66	0.81	2.77	0.84	4.6	0.6	0.46	0.06
M77-4	134	Nearshore	64	-6.00	-85.83	499	27.03	7.7	34.62	6.4	0.05	42.51	0.01	3.13	0.96	4.8	0.6	0.48	0.06
M77-4	134	Nearshore	64	-6.00	-85.83	744	27.24	5.9	34.56	34.9	0.05	44.28	0.01	3.18	0.96	3.1	0.6	0.31	0.06
M77-4	134	Nearshore	63	-6.00	-85.83	995	27.38	4.7	34.56	54.8	0.05	43.59	0.01	3.20	0.95	3.6	0.6	0.36	0.06
M77-4	134	Nearshore	63	-6.00	-85.83	1236	27.49	3.8	34.57	77.6	0.05	41.82	0.00	3.07	0.98	3.4	0.6	0.34	0.06
M77-4	134	Nearshore	63	-6.00	-85.83	1487	27.59	3.1	34.61	82.9	0.05	41.82	0.00	3.04	0.98	2.6	0.6	0.26	0.06
M77-4	134	Nearshore	63	-6.00	-85.83	2962	27.76	1.8	34.68	130.6	0.04	37.19	0.01	2.69	0.88	2.6	0.6	0.26	0.06
M77-4	134	Nearshore	63	-6.00	-85.83	3453	27.76	1.8	34.68	135.3	0.04	37.58	0.01	2.65	0.88	4.4	0.6	0.44	0.06
M77-4	134	Nearshore	63	-6.00	-85.83	3942	27.76	1.8	34.68	136.5	0.04	37.39	0.01	2.66	0.87	4.2	0.6	0.42	0.06

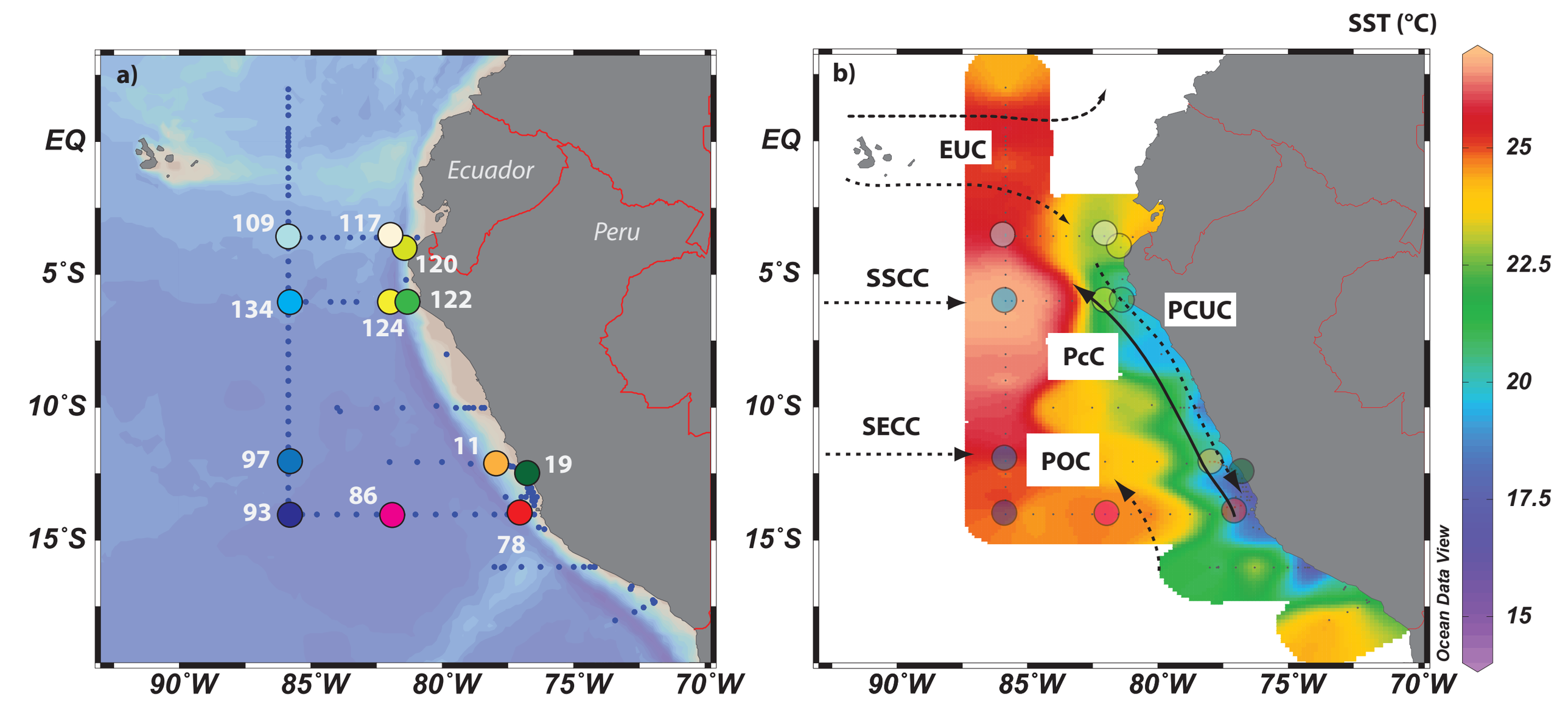
a)
b)
EQ
5˚S
10˚S
15˚S
90˚W
85˚W
80˚W
75˚W
70˚W
Ecuador
Peru
109
117
120
134
122
124
97
11
19
86
93
78
EUC
SSCC
SECC
PCUC
PcC
POC
SST (°C)
25
22.5
20
17.5
15
Ocean Data View

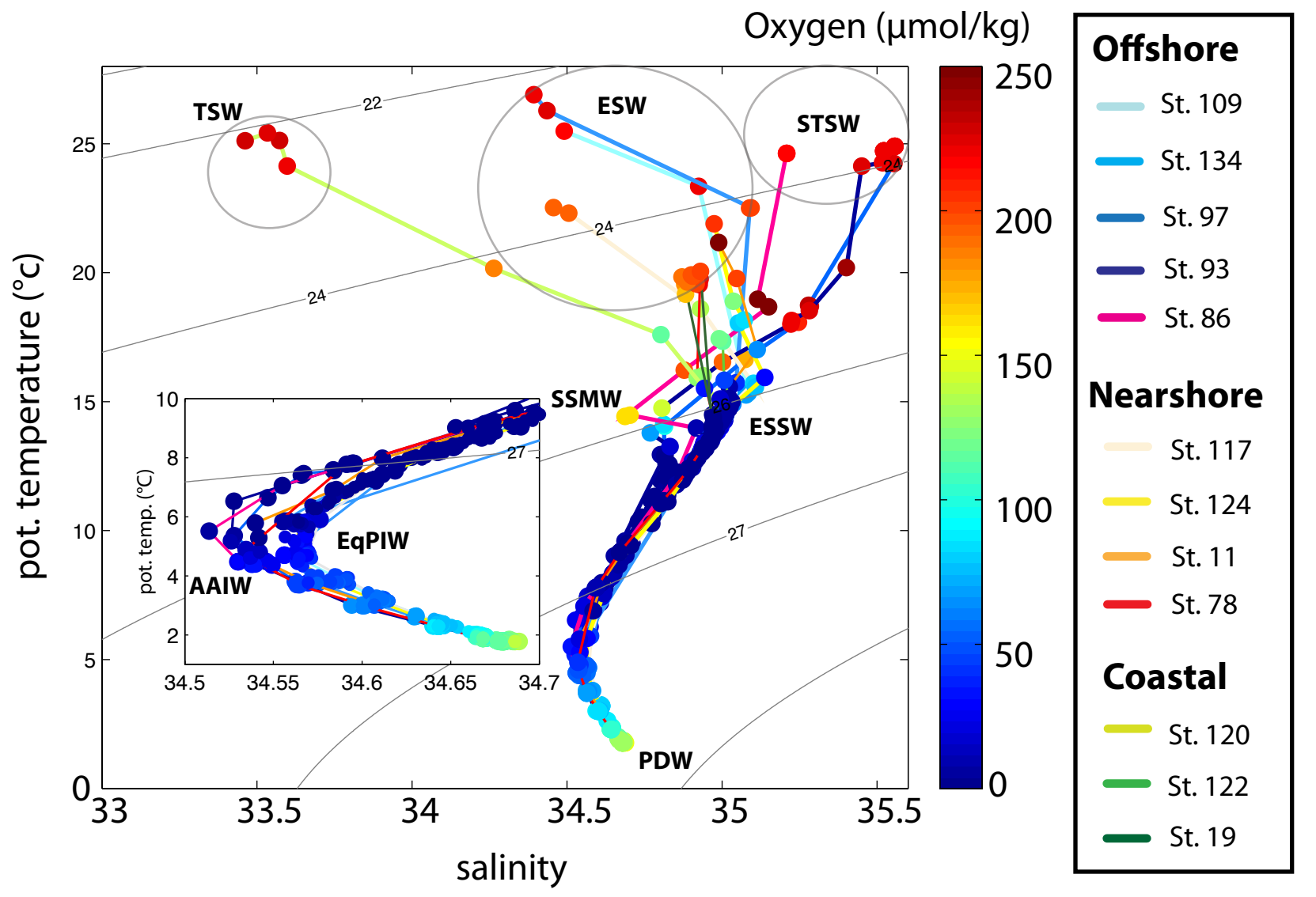
Oxygen (µmol/kg)
250
200
150
100
50
0
pot. temperature (°c)
salinity
0
5
10
15
20
25
33
33.5
34
34.5
35
35.5
TSW
ESW
STSW
SSMW
ESSW
PDW
22
24
24
24
26
27
pot. temp. (°C)
EqPIW
AAIW
2
4
6
8
10
34.5
34.55
34.6
34.65
34.7
27
Offshore
St. 109
St. 134
St. 97
St. 93
St. 86
Nearshore
St. 117
St. 124
St. 11
St. 78
Coastal
St. 120
St. 122
St. 19

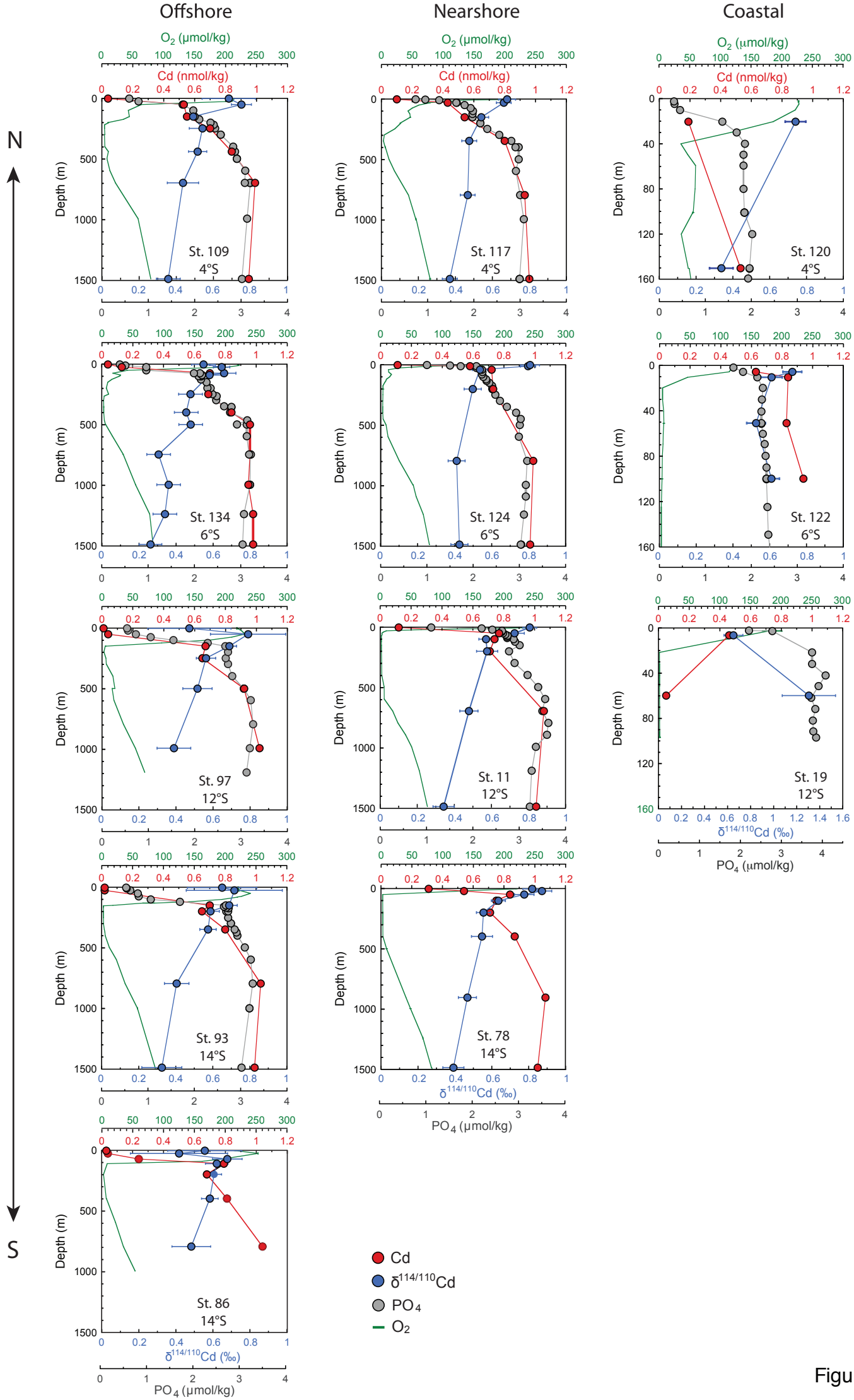
Offshore
Nearshore
Coastal
N
S
O_2 (µmol/kg)
Cd (nmol/kg)
Depth (m)
St. 109
4°S
St. 117
4°S
St. 120
4°S
St. 134
6°S
St. 124
6°S
St. 122
6°S
St. 97
12°S
St. 11
12°S
St. 19
12°S
St. 93
14°S
St. 78
14°S
St. 86
14°S
$\delta^{114/110}$Cd (‰)
PO_4 (µmol/kg)
Cd
$\delta^{114/110}$Cd
PO_4
O_2

Figure 3

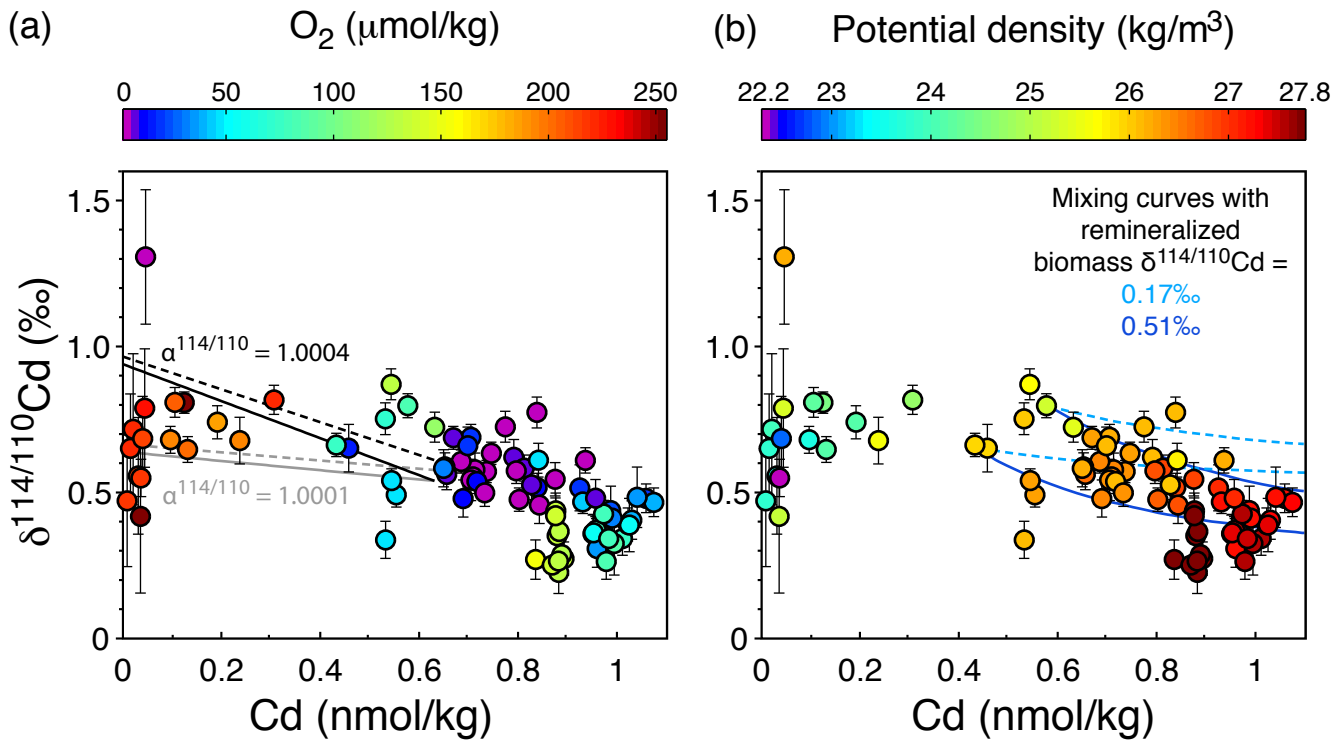
(a)
O2 (μmol/kg)
0
50
100
150
200
250
(b)
Potential density (kg/m3)
22.2
23
24
25
26
27
27.8
δ114/110Cd (‰)
α114/110 = 1.0004
α114/110 = 1.0001
Cd (nmol/kg)
Mixing curves with remineralized biomass δ114/110Cd =
0.17‰
0.51‰
Cd (nmol/kg)

Figure 4

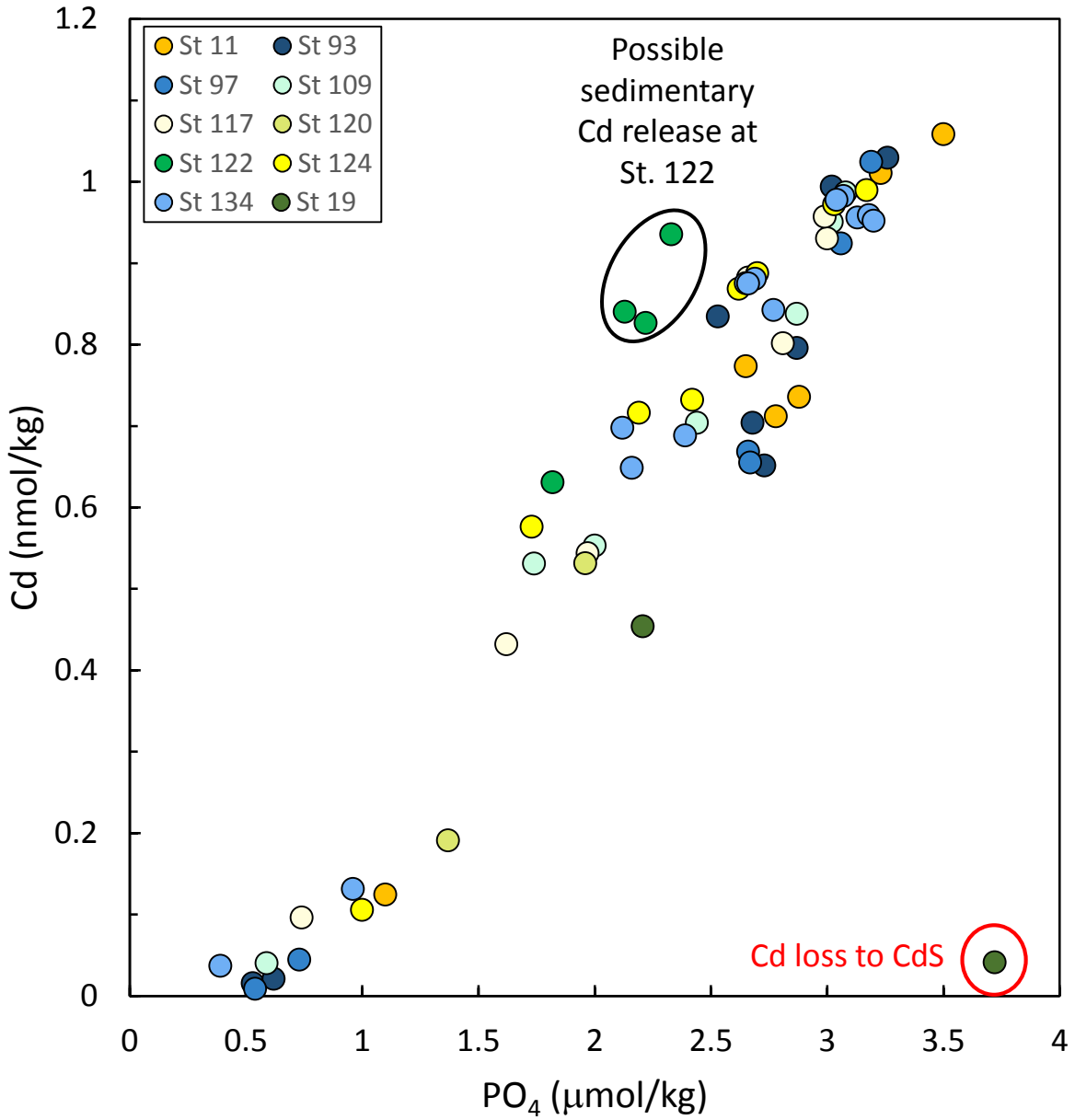
St 11
St 93
St 97
St 109
St 117
St 120
St 122
St 124
St 134
St 19
Possible sedimentary Cd release at St. 122
Cd loss to CdS
Cd (nmol/kg)
PO4 (µmol/kg)
0
0.2
0.4
0.6
0.8
1
1.2
0.5
1.5
2
2.5
3
3.5
4

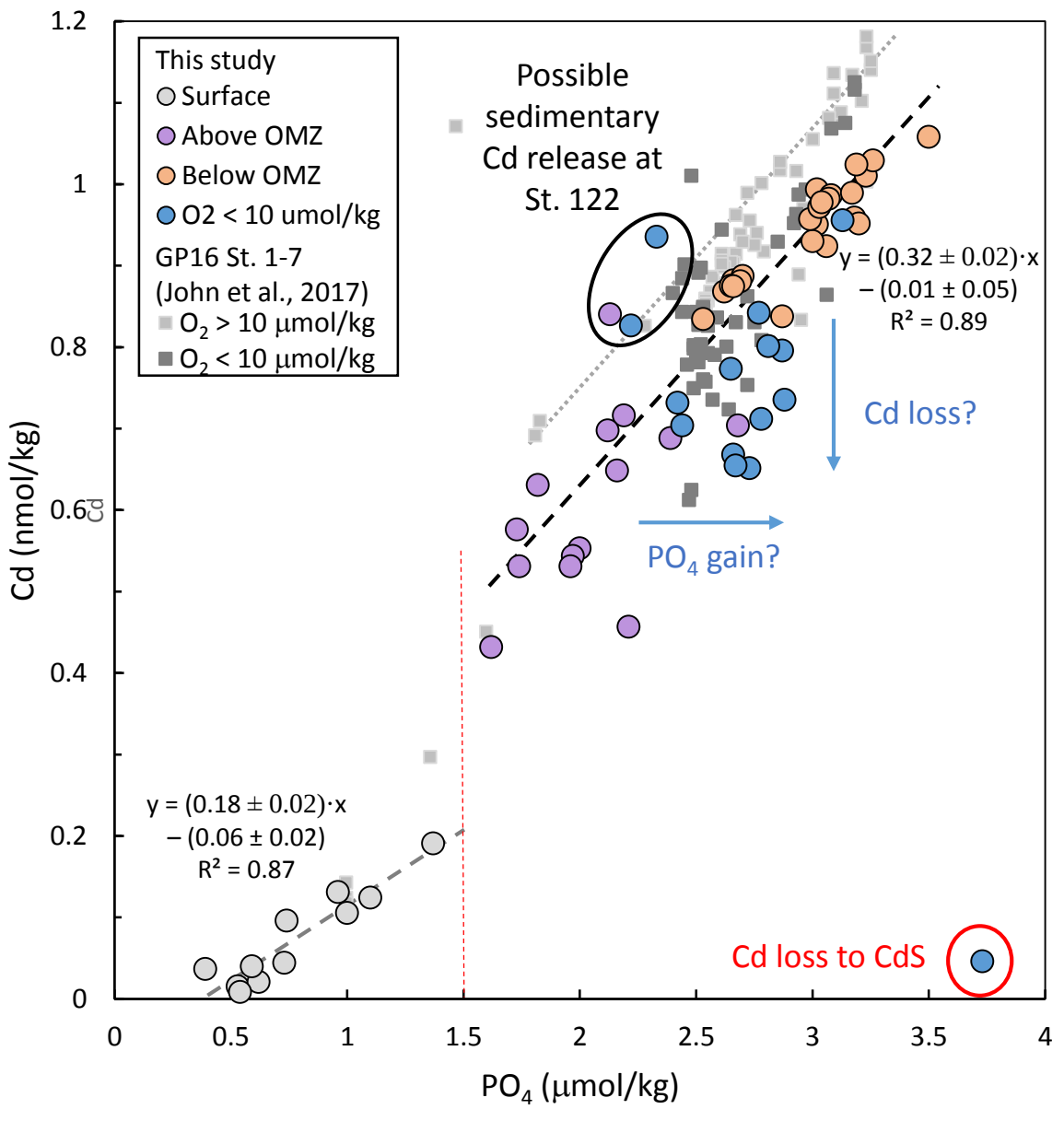
This study
Surface
Above OMZ
Below OMZ
O2 < 10 umol/kg
GP16 St. 1-7
(John et al., 2017)
O2 > 10 µmol/kg
O2 < 10 µmol/kg
Possible sedimentary Cd release at St. 122
y = (0.32 ± 0.02)·x
– (0.01 ± 0.05)
R² = 0.89
Cd loss?
PO4 gain?
y = (0.18 ± 0.02)·x
– (0.06 ± 0.02)
R² = 0.87
Cd loss to CdS
Cd (nmol/kg)
PO4 (µmol/kg)
0
0.2
0.4
0.6
0.8
1
1.2
0.5
1.5
2
2.5
3
3.5
4

Figure 5

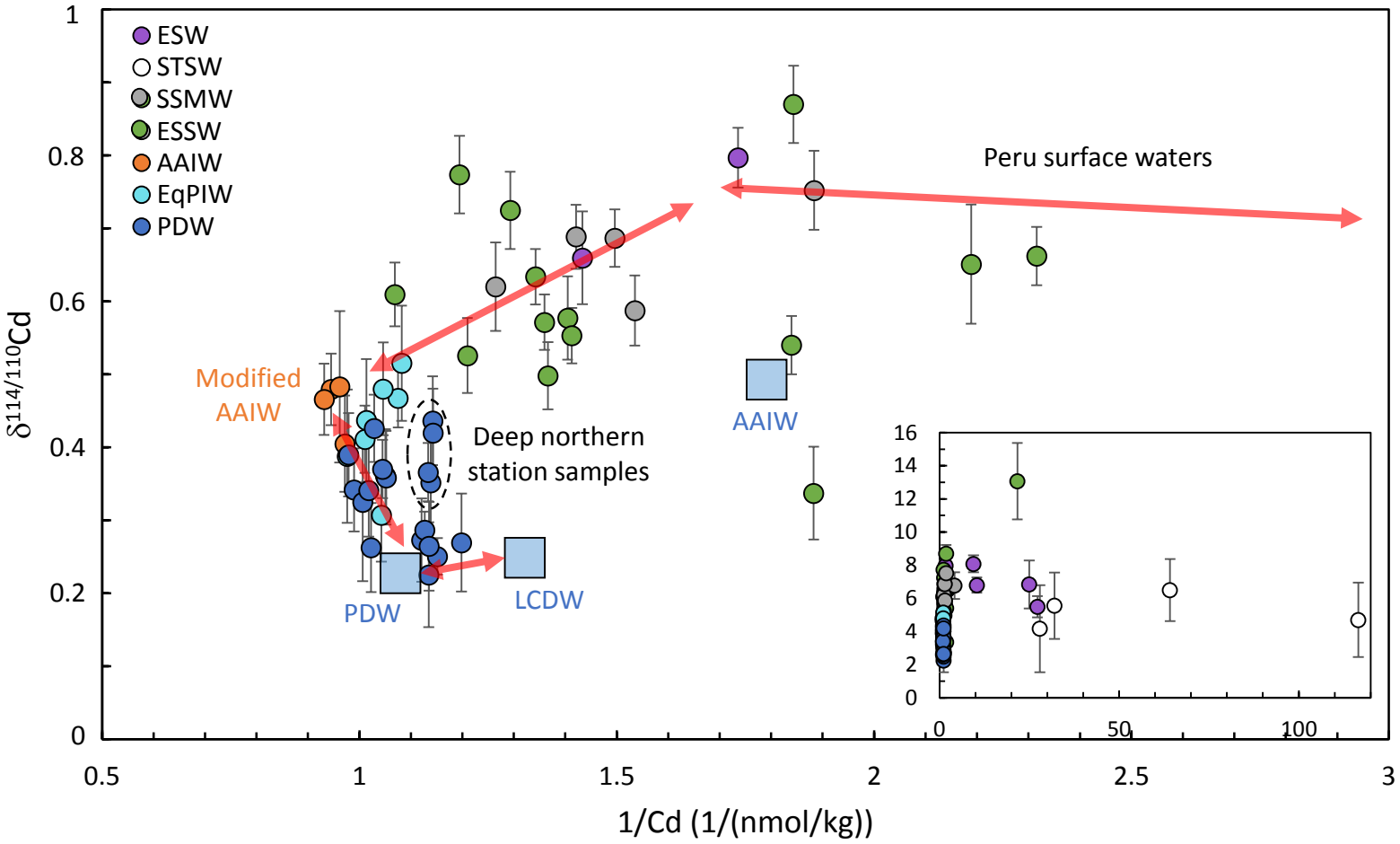
ESW
STSW
SSMW
ESSW
AAIW
EqPIW
PDW
Modified AAIW
Deep northern station samples
PDW
LCDW
AAIW
Peru surface waters
δ114/110Cd
1/Cd (1/(nmol/kg))
0
0.2
0.4
0.6
0.8
1
0.5
1
1.5
2
2.5
3
0
2
4
6
8
10
12
14
16
0
50
100

Figure 6